Received: 27 September 2025 | Revised: 26 January 2026 | Accepted: 27 February 2026

DOI: 10.1002/suco.70552

ARTICLE

fib CEB-FIP WILEY

TRM-to-concrete interface bond without anchors: Combined experimental, analytical, and numerical modeling approach

Ömer Mercimek[1] | **Özlem Çalışkan**[2] | **Özgür Anıl**[3] | **R. Tuğrul Erdem**[4] | **Murat Yüncüler**[2]

[1]Department of Civil Engineering, Ankara University, Ankara, Türkiye

[2]Department of Civil Engineering, Bilecik Şeyh Edebali University, Bilecik, Türkiye

[3]Department of Civil Engineering, Gazi University, Ankara, Türkiye

[4]Department of Civil Engineering, Manisa Celal Bayar University, Ankara, Türkiye

Correspondence
Ömer Mercimek, Department of Civil Engineering, Ankara University, Ankara, Türkiye.
Email: omercimek@ankara.edu.tr

Funding information
Bilecik Şeyh Edebali Üniversitesi, Grant/Award Number: 2022-02. BŞEÜ.01-01; Gazi Üniversitesi, Grant/Award Number: FPD-2024-8919

Abstract

Textile reinforced mortar (TRM) systems have emerged as an effective alternative to conventional FRP strengthening solutions due to their compatibility with concrete substrates and favorable performance under adverse environmental conditions. Experimental data on the combined effects of strip width, bond length, and concrete compressive strength on TRM–concrete bond behavior, however, remain limited. In this study, an experimental program comprising 12 specimens was conducted to investigate the bond–slip response of TRM systems bonded to concrete substrates with two compressive strength classes (15 and 30 MPa), two strip widths (50 and 100 mm), and three bond lengths (150, 300, and 450 mm). The results show that increasing the TRM strip width from 50 to 100 mm significantly enhanced the maximum load capacity by up to 61% in 15 MPa concrete and up to 50% in 30 MPa concrete, depending on the bond length. Increasing the concrete compressive strength from 15 to 30 MPa resulted in maximum load increases of up to 32%, accompanied by a pronounced improvement in stiffness, which increased by over 100% for specimens with 100 mm strip width and 300 mm bond length. Energy absorption capacity was strongly influenced by both strip width and concrete strength. For specimens with 100 mm strip width and 300 mm bond length, increasing the concrete strength from 15 to 30 MPa led to a 61% increase in energy dissipation, indicating improved damage control at the TRM–concrete interface. While increasing the bond length significantly improved load capacity and energy dissipation, diminishing gains were observed beyond a bond length of 300 mm, suggesting the presence of an effective bond length for TRM systems.

Based on the experimental findings, empirical regression models were developed to describe the bond–slip behavior and to define the parameters required for cohesive zone modeling of the TRM–concrete interface. The presented results provide quantitative insights that can support experimental interpretation and numerical modeling of TRM-strengthened reinforced concrete elements.

KEYWORDS

bond–slip behavior, concrete substrate, digital image correlation, experimental study, textile reinforced mortar

1 | INTRODUCTION

The strengthening of existing building stock has become a major research focus in recent years. Fiber-reinforced polymer (FRP) systems have been widely used for this purpose due to their high strength-to-weight ratio, corrosion resistance, and ease of installation. However, the use of epoxy adhesives in FRP systems presents several disadvantages,[1] including poor fire resistance,[2] incompatibility with wet substrates,[3] difficulties in layer replacement, environmental and disposal concerns, limited vapor permeability, and high cost.[4] To overcome these limitations, inorganic mortar matrices have been introduced, giving rise to Textile Reinforced Mortar (TRM) systems. In these systems, open-weave textiles are employed to enhance fiber–matrix interaction, as fine-grained mortars do not fully impregnate continuous fiber sheets. These systems are referred to as TRM or textile reinforced concrete (TRC) in the literature, and as fabric-reinforced cementitious matrix (FRCM) in the United States.[1]

TRM is a composite strengthening material formed by embedding high-strength fiber textiles in an open mesh configuration into cement-based or hydraulic lime-based inorganic mortar. These systems are cost-effective, worker-friendly, fire-resistant, compatible with existing concrete and masonry substrates, and applicable even in damp environments and at low temperatures. Consequently, TRM has emerged as an advantageous external strengthening method, especially in historical masonry structures or environments with fire risks, where epoxy-based FRP systems have limitations. Recent studies have significantly explored the use of TRM systems in strengthening reinforced concrete (RC) structures. Research efforts have focused on improving the flexural behavior of RC elements,[5–10] enhancing shear capacity,[11–19] increasing the axial load capacity and seismic performance of RC columns through confinement.[3,20–27] However, studies investigating the bond and bond–slip behavior between TRM composites and concrete surfaces remain relatively limited.[28] A detailed investigation of the interfacial bond between TRM systems and concrete substrates is crucial since such research helps elucidate the complex mechanisms involved in load transfer from textile reinforcement to mortar and ultimately to the concrete substrate. Moreover, comprehensive investigations in this field are fundamental for developing design models to be used in strengthening applications.

The effectiveness of TRM systems bonded to concrete surfaces with mortar largely depends on the interfacial bond behavior. To ensure successful load transfer after strengthening, the bond strength between TRM and concrete substrates is critical. The mortar layer facilitates stress transfer between the concrete surface and textile reinforcement. Under tensile forces, shear stresses develop at the interface, and the composite works together cohesively up to a certain load level. Typically, at low load levels, the TRM–concrete interface remains slip-free (full adhesion), and the load-carrying system exhibits high initial stiffness.[28] With increasing load, initial cracks form within the mortar, initiating a nonlinear phase marked by reduced stiffness in the bond curve.[28] Prior to reaching ultimate capacity, multiple cracking occurs throughout the mortar, distributing stresses along the textile reinforcement. Subsequently, the bond mechanism exhibits sudden or gradual stress reduction, depending on the failure modes.

Two primary types of debonding modes at the TRM–concrete interface have been reported in the literature: (a) slippage of textile fibers within the mortar (matrix slippage), and (b) separation of the TRM layer from the concrete substrate (interface debonding).[5] In the first case, fiber bundles constituting the textile reinforcement begin to slip out of the mortar due to friction, resulting in a gradual reduction in load-carrying capacity without dropping to zero completely. Friction and mechanical interlocking between fibers and mortar provide residual strength, preventing abrupt brittle failure. Indeed, TRM

systems with a single layer or a low reinforcement ratio typically exhibit this type of ductile bond-slip behavior with residual capacity. In the second case, the adhesion between the mortar layer and the concrete substrate fails suddenly, causing complete separation of the TRM coating from the concrete, typically occurring at peak load and resulting in an immediate and sharp drop in load-carrying capacity. In multi-layered or high-strength mortar TRM applications, interface stresses are higher, and brittle failure may occur as separation from the concrete substrate or peeling of the concrete cover, resembling the typical concrete cover separation mode observed in epoxy-bonded FRP systems. However, fiber slippage within mortar is more common in TRM systems, providing more ductile adhesion behavior compared to FRP. Additionally, due to the inorganic composition of TRM, it outperforms FRP in adhesion performance under extreme conditions such as high temperatures, where cement-based TRM systems retain bonding capability, unlike epoxy binders that soften and lose strength.[1] However, it has also been noted in some studies that early slippage at the fiber–matrix interface in TRM systems prevents fibers from reaching their ultimate tensile strength, thus theoretically resulting in slightly lower ultimate load-carrying capacities compared to FRP systems with equivalent reinforcement ratios. Overall, several variables affect the debonding mode (number of textile layers, fiber type, mortar properties, surface preparation, etc.), and their effects are summarized below based on findings from the literature.

The bond behavior of TRM and FRCM systems on concrete has been extensively investigated, emphasizing the influence of bond length, number of layers, fiber type, matrix properties, surface preparation, and anchorage on interfacial performance. Raoof et al.[28] found that bond lengths beyond 200–300 mm provide limited strength gains, additional TRM layers increase adhesion nonlinearly and modify failure modes, and both epoxy-coated textiles and end anchorage enhance load capacity. D'Ambrisi et al.[29] similarly reported that PBO-FRCM systems debond after significant fiber–matrix slippage, identifying an effective anchorage length of approximately 250–300 mm for single-layer applications, supporting the development of local bond–slip relationships. D'Antino et al.[30] highlighted the critical role of fiber type and matrix interaction, observing that carbon and glass fibers fail mainly by slippage while steel fibers separate completely, with carbon fiber bonding improving with matrix strength and glass fibers exhibiting a telescopic mechanism during damage progression. More recently, Zhang et al.[31] demonstrated that adding short fibers to carbon TRM systems significantly enhances bond strength, crack control, and load-carrying capacity, with textile geometry, layer number, and impregnation methods further affecting interface behavior, leading to a comprehensive bond–slip model for short-fiber-reinforced TRM systems. Collectively, these studies underscore the fundamental roles of bond length, fiber–matrix interaction, and material configuration in optimizing TRM and FRCM strengthening performance.

Single-lap shear tests conducted by Ombres[32] revealed that adhesion between PBO fiber-based FRCM systems and concrete primarily deteriorated at the fiber–matrix interface, influenced by factors like bond length, textile layers, and environmental conditions such as high temperatures. Similarly, D'Antino et al.[33] reported that concrete surface preparation and strength significantly influence fiber–matrix interface debonding in FRCM composites, emphasizing the necessity of adequate surface preparation and matrix shrinkage control to prevent sudden, brittle failures. Awani et al.[34] compared mortar-based FRCM systems with epoxy-based systems through double shear tests, indicating that fabric slippage from the matrix was the dominant failure mode in mortar-based samples, resulting in lower bond stresses compared to epoxy systems. Tran et al.[35] found through single tensile tests that the effective bond length in PBO–FRCM systems is significantly longer than in traditional FRP systems, primarily due to widespread microcracking in cementitious matrices, enlarging the load transfer zone. Sneed et al.[36] demonstrated via single-lap shear tests that bond strength in FRCM composites is unaffected by width, unlike FRP systems, and damage propagates differently along fiber–matrix interfaces on both sides of textile reinforcement.

Following the devastating earthquakes in Türkiye on February 6, 2023,[37] numerous studies have been conducted to assess the structural damage observed in RC buildings.[38–43] Several of these investigations also propose various strengthening strategies to mitigate future seismic vulnerabilities. In parallel, recent research has emphasized the complexity of the bond behavior between TRM and concrete, highlighting the necessity for detailed investigations to develop reliable strengthening design models. However, studies addressing key parameters, such as TRM strip width and the influence of varying concrete compressive strengths, remain scarce. The present study aims to fill these critical gaps by systematically examining the effects of different bond lengths (150, 300, and 450 mm), strip widths (50 and 100 mm), and low-to-normal concrete strength classes. The findings provide essential insights for refining existing design guidelines and enhancing the effectiveness of TRM-based strengthening solutions in earthquake-prone regions.

2 | EXPERIMENTAL STUDY

The experimental program presented in this study is based on a set of 12 TRM-to-concrete specimens previously tested and reported in Çalışkan et al.,[44] which focused on the effect of fan-type mechanical anchors. In the present study, only the unanchored specimens from that experimental matrix are considered, and their detailed geometrical and material properties, as well as individual test results, were previously published. To avoid redundancy, only key parameters are summarized herein, while a comprehensive description of specimen fabrication, instrumentation, and boundary conditions can be found in the referenced publication.

2.1 | Details of specimens

In this experimental study, a total of 12 specimens were prepared to investigate the bond behavior of TRM strips with concrete surfaces. The study specifically examined the variables of TRM strip width, bond length, and concrete compressive strength. Specimens were produced using two different concrete strength classes: low-strength concrete (15 MPa) and normal-strength concrete (30 MPa). For each concrete strength class, TRM strip widths were set at 50 and 100 mm, while the bond lengths for attaching the strips to concrete surfaces were selected as 150, 300, and 450 mm, respectively. This enabled a comprehensive evaluation of various parameters. The naming of specimens, along with detailed information on concrete strengths, TRM strip widths, and bond lengths, is clearly presented in Table 1. Additionally, schematic representations illustrating the geometric characteristics, dimensions, and general layout details of the specimens are provided in Figure 1. The primary aim of examining these combined parameters—bond lengths, strip widths, and concrete strength—is to achieve a clearer understanding of the adhesion mechanisms at the TRM–concrete interface.

The parameters investigated in this study were selected based on existing gaps in the literature and significant findings highlighted in previous research. The choice of bond lengths (150, 300, and 450 mm) was inspired by previous studies emphasizing the critical nature of effective bond length and load transfer mechanisms in TRM systems.[35] The strip width parameter emerged as a topic frequently overlooked and not thoroughly investigated in earlier studies. There is a notable gap in the literature, particularly regarding the influence of strip width on bond stress distribution and load-carrying capacity.[36] Concrete compressive strength was chosen based on findings by D'Antino et al.,[30] which emphasized the influence of concrete surface preparation and concrete strength on the bond behavior of TRM systems. Consequently, two classes—low (15 MPa) and normal (30 MPa)—were selected to comparatively investigate the impact of weak and moderate-strength concrete substrates on the bond mechanism.

2.2 | Prefabrication of specimens

The production of experimental specimens was carried out in three main stages: preparation of concrete specimens, bonding of TRM strips onto concrete surfaces, and

TABLE 1 Properties of specimens.

			Textile reinforced mortar strip	
Spec. #	**Name**	**Compressive strength of concrete (MPa)**	**Width (mm)**	**Bonding length (mm)**
1	C15-W50-L150	15	50	150
2	C15-W50-L300			300
3	C15-W50-L450			450
4	C15-W100-L150		100	150
5	C15-W100-L300			300
6	C15-W100-L450			450
7	C30-W50-L150	30	50	150
8	C30-W50-L300			300
9	C30-W50-L450			450
10	C30-W100-L150		100	150
11	C30-W100-L300			300
12	C30-W100-L450			450

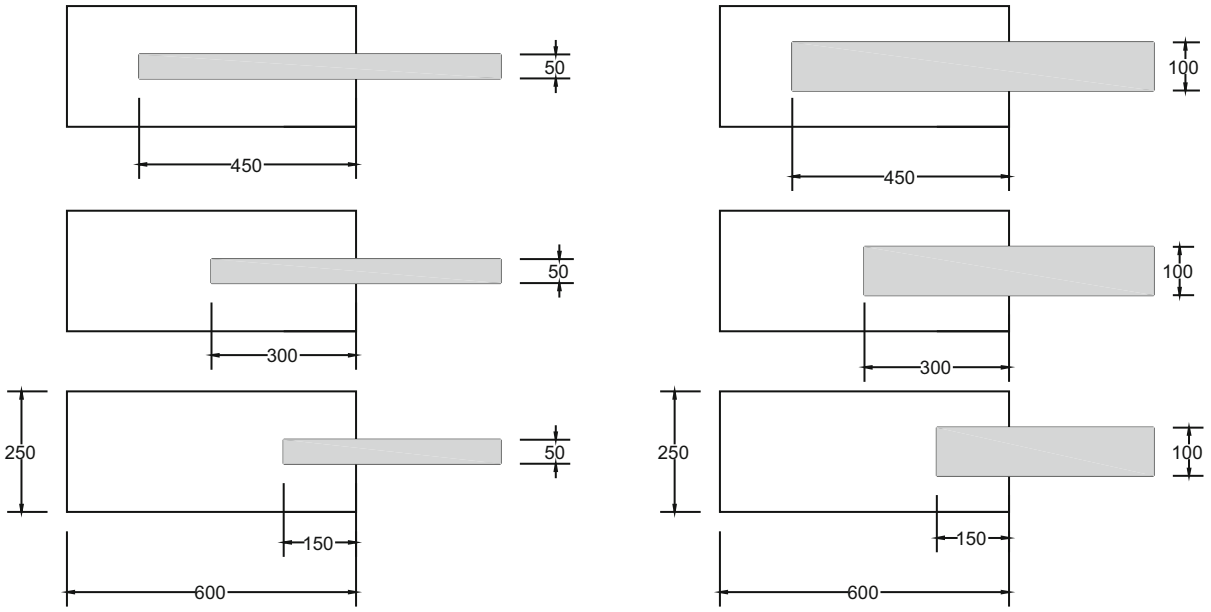

FIGURE 1 Geometric details of specimens.

FIGURE 2 Production of concrete for test specimens.

surface preparation for digital image correlation (DIC) analysis.

In the first stage, wooden molds were meticulously prepared to ensure accurate geometry and dimensions of the experimental specimens (Figure 2). The smoothness and robustness of these molds are crucial for the dimensional consistency of the specimens. After mold preparation, fresh concrete mixed according to the designed

FIGURE 3 Bonding procedure of TRM strip to concrete surface.

strength was poured into the molds. Following casting, the concrete surfaces were carefully smoothed to provide a uniform and homogeneous bonding surface for the strips. Additionally, specially designed steel rings were embedded in the concrete to facilitate transportation and lifting. The smoothness and surface quality of the concrete were given careful attention, as they directly influence the bond performance between the TRM and concrete (Figure 2).

After completing an adequate curing period for the concrete specimens, the second stage involved surface preparation for bonding the TRM strips. Initially, concrete surfaces were mechanically ground and roughened, providing the necessary adhesion area for stronger bonding of the TRM strips to the concrete (Figure 3). Concrete surface preparation was carried out using mechanical grinding with a rotating disc rather than sandblasting or shot blasting techniques. Mechanical surface grinding using a rotating disc was selected instead of sandblasting or shot blasting, as it provides a more homogeneous and controllable concrete surface. In contrast, sandblasting and shot blasting may induce irregular voids and weak zones due to aggregate pull-out, microcracking, and the formation of a locally weakened surface layer, particularly in normal- and low-strength concretes. Furthermore, mechanical grinding can be applied more easily under laboratory conditions, does not require specialized equipment, and ensures a high level of

repeatability, which is essential for achieving consistent and comparable bond test results. Following surface grinding, dust and particles generated on the concrete surfaces were cleaned using compressed air, ensuring the bonding area was free from any adhesion-reducing contaminants. Carbon-based textile reinforcements were carefully cut according to the designed dimensions. Following the cutting of the carbon textiles, the carbon textile mesh strips were coated with mortar. In order to delay debonding of the carbon textiles from the concrete surface, a high-performance fiber-reinforced repair mortar was used instead of conventional plaster mortars. As recommended by the manufacturer, the 25-kg bag of dry mix was gradually poured into a container containing 4 L of water and mixed mechanically until a homogeneous mortar was obtained. The prepared mortar was then uniformly applied to the carbon textile strips, and the surface was finished using a wet sponge to achieve a smooth layer. Owing to the 25 × 25 mm openings in the carbon textile mesh, the mortar could easily penetrate and adhere to both the upper and lower faces of the strips, thereby ensuring effective bonding between the strips and the concrete specimens. To allow the applied mortar to gain sufficient strength and to complete the strengthening process, the mortar-coated regions were cured by water spraying for 7 days, followed by storage under laboratory conditions for an additional 21 days, completing a total curing period of 28 days (Figure 3).

In the final stage, the DIC technique was employed to accurately and precisely measure the bond mechanism on the adhered TRM strips. Proper surface preparation of the TRM strips was critically important for the effectiveness of the DIC analysis. For this purpose, the upper surfaces of the TRM strips were ground again to create smooth and homogeneous surfaces suitable for point cloud data acquisition using the DIC method (Figure 4). Subsequently, the perimeters of the strips were protected by taping to ensure clear and error-free image acquisition, followed by a painting procedure. This provided a uniform texture with sufficient contrast on the surface, enhancing the accuracy of the image correlation. These preparations enabled high-precision measurement of deformation and slip amounts occurring on the specimen surfaces during testing (Figure 4).

FIGURE 4 Preparations for DIC.

2.3 | Materials

In this study, carbon-based textile reinforcement along with special fiber-reinforced high-performance mortar was used for strengthening concrete surfaces (Table 2). Detailed technical specifications, mechanical performances, and reasons for selecting these materials and concrete are presented below.

2.3.1 | Concrete

The concrete specimens were produced using ready-mixed concrete with nominal strength classes of C15 and C30, supplied by a certified batching plant. Since ready-mixed concrete was used, the exact mix proportions were determined by the producer and were not designed within the scope of this study.

In order to verify the mechanical properties of the concrete, standard cube specimens were collected from each mixer truck and tested in compression in accordance with relevant standards.[45] The test results confirmed that the measured compressive strengths were consistent with the target strength classes, thereby validating the use of C15 and C30 concrete in the experimental program.

2.3.2 | Carbon textile

The carbon-based textile reinforcement selected for strengthening in this experimental study is Carbon-350, manufactured from high-strength and high-rigidity carbon fibers. This material provides superior mechanical performance. With an area weight of 350 g/m^2, it ensures ease of application and minimal additional load on the structure. The tensile strength of the carbon textile was measured as 255 kN/m, providing the high strength necessary for structural strengthening applications. The thickness of 1.43 mm ensures no functional impairment upon application to concrete surfaces, while its modulus of elasticity was determined as 235 GPa. This high modulus significantly enhances the load-carrying capacity of the strengthening system and reduces deformation by limiting crack formation. Its rupture elongation of 1.7% offers the advantage of ductile behavior rather than brittle, preventing sudden failure and enhancing structural safety.

TABLE 2 Mechanical properties of materials.[a]

Technical specifications of carbon textile material		
Fiber type	Carbon-350	
Tensile strength (kN/m)	255	
Weight (g/m^2)	350	
Thickness (mm)	1.43	
Elastic modulus (GPa)	235	
Failure strain (%)	1.7	
Technical specifications of special fiber added mortar		
Flexural strength (MPa)		28 days: >8.0 N/mm^2
Bonding strength (MPa)		>2 N/mm^2
Compressive strength (MPa)		1 days: >30 N/mm^2 7 days: >50 N/mm^2 28 days: >60 N/mm^2

[a]Properties were obtained from the manufacturer.

2.3.3 | Special fiber-reinforced repair mortar

Special fiber-reinforced high-performance repair mortar was used to effectively bond TRM systems to concrete surfaces and ensure sufficient mechanical performance. This mortar, enhanced by special fibers, prevents crack formation and significantly increases strength. According to data provided by the manufacturer, the mortar exhibits a flexural strength exceeding 8 MPa after 28 days, which is critical for resisting tensile stresses induced by applied loads.

The adhesion strength between the mortar and concrete surface was measured at over 2 MPa, ensuring effective and continuous load transfer through integration with the concrete substrate. Additionally, the mortar's high adhesion strength prevents debonding and separation from the concrete surface throughout the service life of the strengthening system.

The compressive strength of the mortar is notably high even at early ages, exceeding 30 MPa within 1 day, thus facilitating rapid site application. Its compressive strength surpasses 50 MPa at 7 days and achieves a final strength above 60 MPa at 28 days. This superior compressive strength significantly enhances the load-carrying capacity and overall durability of the strengthened concrete elements, positively impacting the long-term performance of the structure.

The outstanding mechanical and physical properties of the carbon textile reinforcement and special fiber-reinforced repair mortar directly enhance the performance of the TRM strengthening system. Specifically, these materials significantly improve the reliability of bond mechanisms with concrete surfaces, load-carrying capacities, and long-term durability. Consequently, the selection of materials was conducted comprehensively and meticulously, aligning with the experimental objectives of the study.

2.4 | Test setup and instrumentations

Within the scope of this study, a specially designed experimental setup was employed to thoroughly investigate the bond–slip behavior between TRM strips and concrete surfaces (Figure 5). The test system was developed based on existing literature and the authors' previous experiences, ensuring accurate and reliable measurement results.

In the experimental setup, axial loading was applied using a hydraulic jack with a capacity of 500 kN. The applied load was continuously monitored using a calibrated load cell with a maximum capacity of 400 kN. Although the maximum capacity of the load cell (400 kN) and the hydraulic jack (500 kN) are significantly higher than the applied loads, which were limited to 16 kN, the load cell was calibrated in accordance with international standards and possesses a suitable accuracy class. Considering the accuracy and resolution of the measurement system, the potential measurement error at low load levels is negligible and does not affect the validity of the experimental results.

To measure the relative slip occurring in the bonding region between the TRM strip and the concrete substrate, a high-precision linear variable differential transformer (LVDT) with a 100 mm measurement range was utilized. The positioning of the LVDT was meticulously designed to measure only the slip at the concrete–TRM interface and exclude any deformation occurring within the TRM strip itself.

The LVDT was securely fixed to the experimental setup using a magnetic base mounted on a rigid support. Its measuring tip was placed in constant contact with a steel attachment fixed to the TRM strip. Thus, the movement of the TRM strip and the relative slip at the interface with the concrete surface could be monitored with high precision during loading. Throughout all experiments, the loading procedure was adjusted such that each test was completed within approximately 1–3 min, ensuring consistent quasi-static loading among all specimens. Although earthquake loading is inherently dynamic, the present experimental approach focuses on the quasi-static response to evaluate structural capacity, stiffness degradation, and failure mechanisms. Quasi-static tests are commonly employed in seismic research to characterize the envelope response and damage evolution of structural elements without the influence of inertial and strain-rate effects. Accordingly, the experimental results are interpreted in the context of seismic performance assessment rather than direct simulation of dynamic earthquake excitation.

All measurements obtained during the experiment were recorded in real-time through a digital data acquisition system, enabling instantaneous monitoring of load–

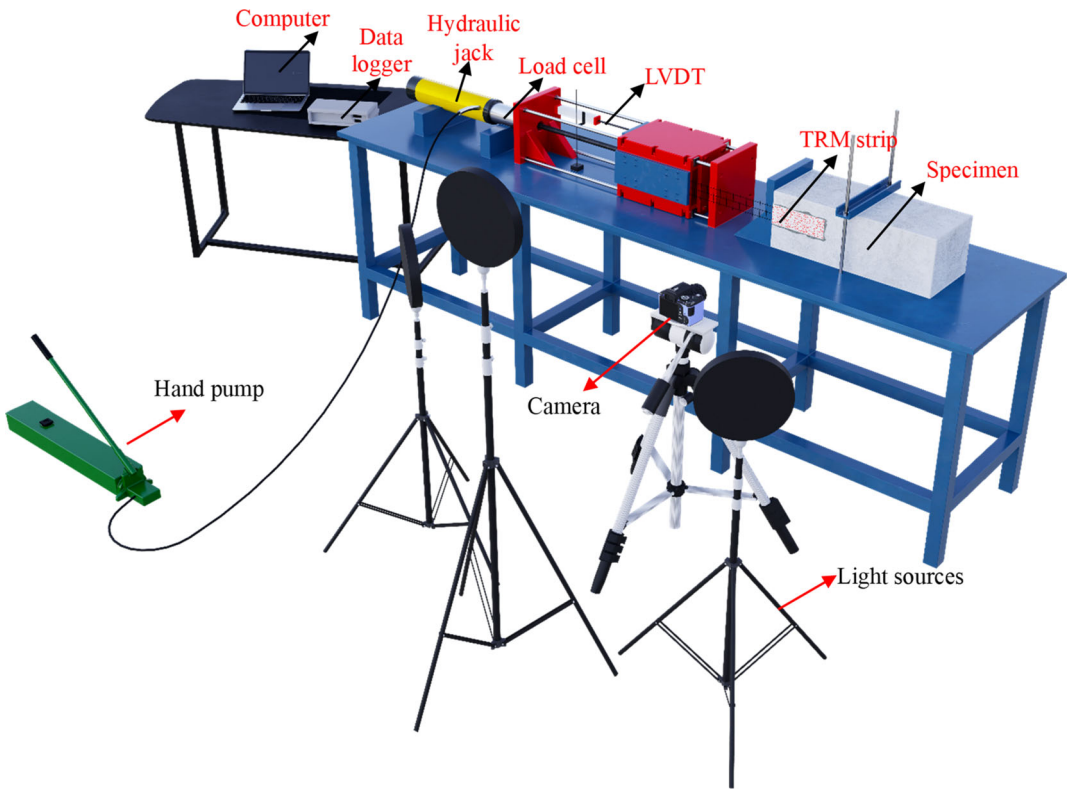

FIGURE 5 Experimental setup.[44]

slip curves throughout the tests. A three-dimensional schematic drawing clearly illustrating the roles of all components of the experimental setup and their interrelationships is presented in Figure 5. Also, the real image of the testing setup is presented in Figure 6. This provides a comprehensive understanding of the details of the experimental arrangement, placement, and functions of the measurement systems.

2.5 | DIC system

DIC is an advanced optical measurement technique that allows contactless measurement of strain and displacement behaviors in materials under load. This method employs sophisticated algorithms to analyze sequential surface images captured before and during deformation, identifying surface deformations at the pixel level. For analysis, specimen surfaces were typically prepared by creating a random speckle pattern using spray paint, ensuring unique and distinctive features necessary for precise tracking of pixel movements during image analysis (Figure 7).

During experiments, high-resolution digital cameras captured specimen surface images at regular time intervals. These images were analyzed using specialized software to calculate displacements and deformations at various points on the material from pixel movements on the surface. The DIC technique offers significant advantages such as high precision in detecting micro-scale deformations, comprehensive surface-wide measurements, and the absence of physical contact with the specimen during measurement.

In this study, the DIC method was utilized to investigate strain distributions on the surfaces of TRM strips bonded to concrete and detailed slip behaviors in the bond region. Images of specimen surfaces were captured every 5 s during the tests using a Canon EOS 700D digital camera positioned perpendicularly to the specimen surfaces. Consistent and homogeneous lighting throughout the experiments was provided by three circular LED light sources with a color temperature of 3000 K, ensuring stable image quality and clarity. The schematic arrangement designed for measuring strain and slip behaviors on specimens using the DIC system is clearly illustrated in Figure 7.

Image analysis was conducted using the open-source Ncorr software,[46] operating within MATLAB.[47] Ncorr software compares the initial and post-deformation states of materials within user-defined regions of interest (ROI) and calculates surface deformations using advanced algorithms. Consequently, data on deformation and displacement behaviors were obtained both numerically and graphically, facilitating a detailed evaluation of strain distributions and local deformations under load.

Critical parameters for ensuring accuracy and consistency in the DIC analysis were carefully determined. The subset radius was selected between 10 and 12 pixels based on image pixel resolution. Additionally, the maximum number of iterations during analysis was consistently fixed at 100 for all specimens. This standardized approach guaranteed reliability and comparability of experimental results.

3 | EXPERIMENTAL RESULTS

In this section, experimental results conducted to evaluate the bond performance between TRM strips and

FIGURE 6 The real configuration of the test setup.

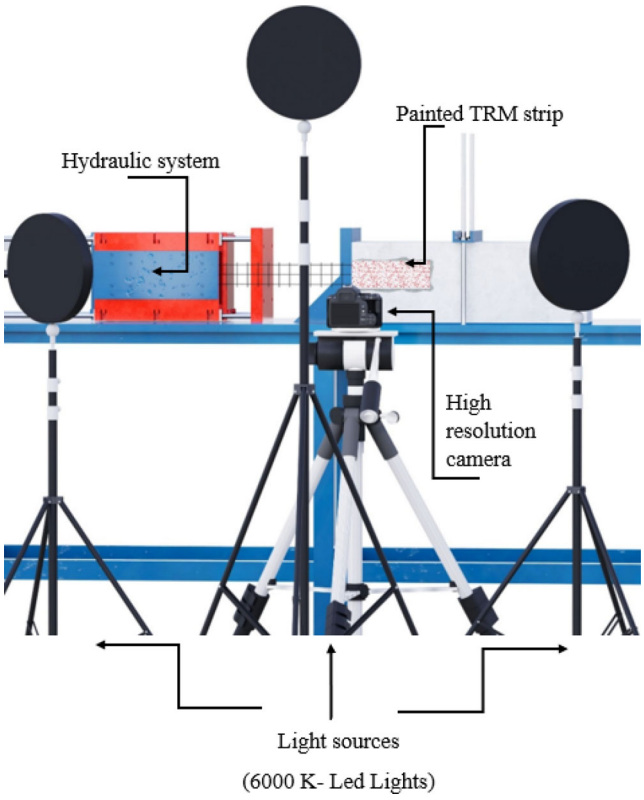

FIGURE 7 Digital image correlation system.[44]

concrete surfaces are comprehensively analyzed and discussed. Load–displacement curves are presented in Figure 8. Structural performance indices such as maximum load-carrying capacity, displacement at maximum load, stiffness, and energy dissipation capacity were calculated using the approaches illustrated in Figure 9. In the load–displacement graphs, the maximum load value is denoted as L_{max}, and the corresponding displacement at this load is recorded as D_{max}. The ratio of L_{max}/D_{max} represents stiffness. The area under the load–displacement curve is calculated as the energy dissipation capacity. The experimental parameters included concrete compressive strength (15 and 30 MPa), strip width (50 and 100 mm), and bond length (150, 300, and 450 mm). The results obtained from the experiments, including maximum load (kN), displacement at maximum load (mm), stiffness (kN/mm), maximum displacement (mm), and energy dissipation (kN·mm), are summarized in Table 3. The experimental outcomes are discussed in detail below, taking into consideration the experimental variables.

3.1 | Max. load capacity and effect of strip length

According to the experimental findings, the maximum load capacity increased with the bond length of the TRM strips (Figure 10). For instance, in specimens with low-strength concrete (15 MPa) and 50 mm wide TRM strips, increasing the bond length from 150 to 300 mm resulted in approximately a 78% increase in maximum load capacity (from 4.06 to 7.23 kN). Further increasing the bond length to 450 mm led to an even greater capacity, reaching a maximum load of 8.11 kN. Similarly, for 100 mm wide strips, extending the bond length from 150 to 450 mm increased the maximum load capacity by approximately 71%, from 6.53 to 11.17 kN. These results indicate a significant yet nonlinear increase in load capacity with increasing bond length, with a notably reduced rate of increase beyond the 300 mm bond length.

Moreover, when the concrete strength was increased to 30 MPa, the maximum load-carrying capacity notably improved at every bond length. For instance, the maximum load for 100 mm wide TRM strips increased from 6.53 to 7.30 kN at a 150 mm bond length and from 9.51 to 12.28 kN at a 300 mm bond length. At a bond length of 450 mm, the maximum load capacity rose from 11.17 to 14.78 kN, clearly highlighting the impact of concrete strength on bond performance.

3.2 | Effect of strip width

One of the critical parameters examined in this study, the TRM strip width, significantly impacted the behavior of the bond mechanism. The increase in strip width emerged as an influential factor affecting both load-carrying capacity and deformation distribution at the TRM–concrete interface. Although this parameter has typically been either minimally investigated or neglected in the existing literature, the results obtained from this study indicate that the effectiveness of strip width may be much higher than previously assumed.

In low-strength concrete specimens (15 MPa), increasing the strip width from 50 to 100 mm at a bond length of 150 mm resulted in an approximately 61% increase in maximum load capacity, rising from 4.06 to 6.53 kN. This trend remained consistent for other bond lengths, with load increases of 32% (from 7.23 to 9.51 kN) at a bond length of 300 mm and 38% (from 8.11 to 11.17 kN) at a bond length of 450 mm. This observation suggests that wider TRM strips increase the contact area with the concrete surface, allowing stress at the interface to be more evenly distributed over a larger area. Consequently, reducing local stress concentrations enhances interface bond strength and the system's overall load-carrying capacity.

In normal-strength concrete specimens (30 MPa), the effect of strip width became even more pronounced. At a bond length of 150 mm, increasing the strip width from 50 to 100 mm increased the maximum load capacity by

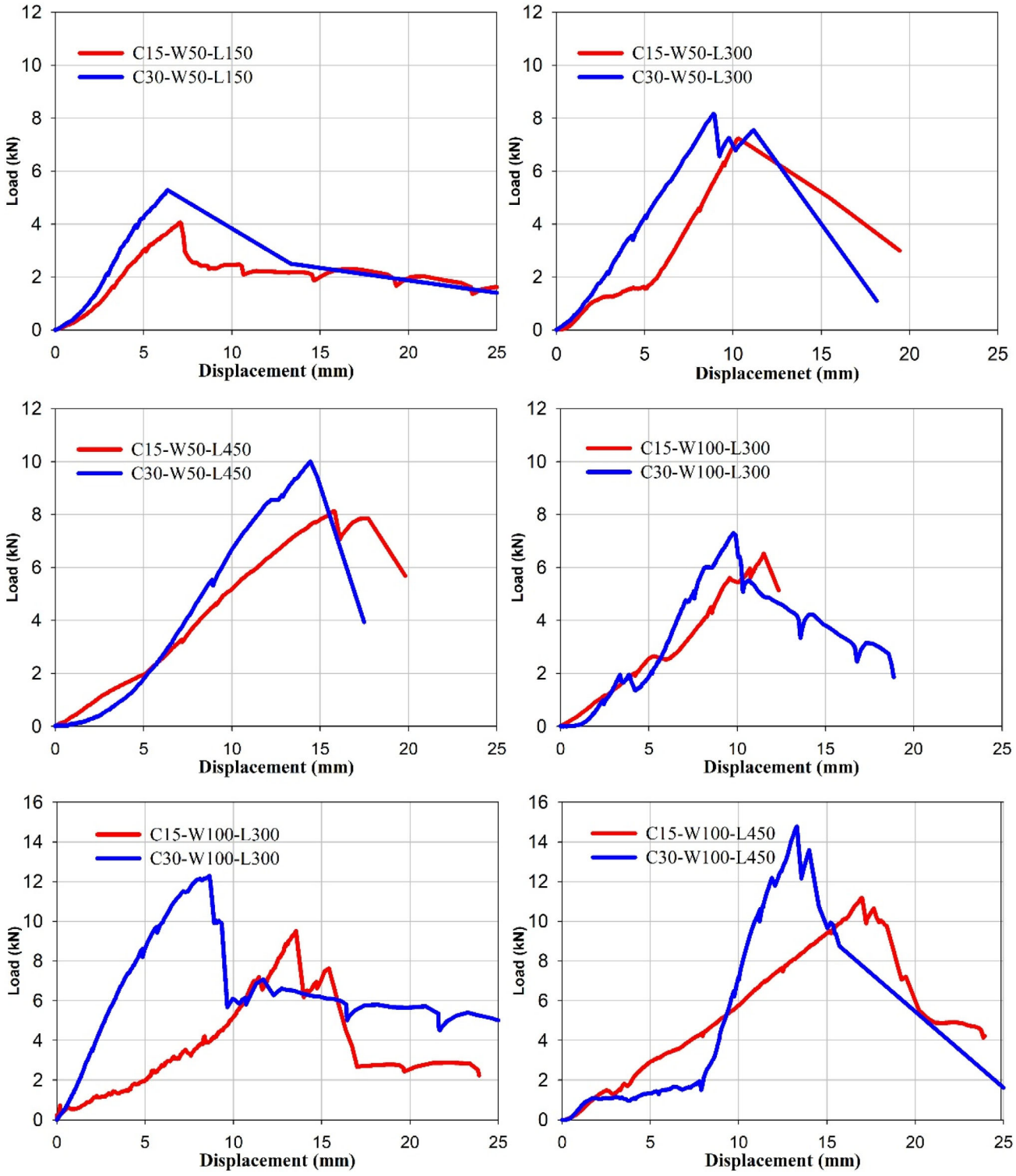

FIGURE 8 Load–displacement curves of specimens with C15–C30 concrete grade.

approximately 38%, from 5.28 to 7.30 kN. This increase was more significant at longer bond lengths: about 50% at 300 mm bond length (from 8.16 to 12.28 kN) and 48% at 450 mm bond length (from 10.01 to 14.78 kN). These results indicate that wider strips effectively utilize the concrete surface, maximizing load transfer capacity, particularly when concrete strength is higher.

Increasing strip width positively affected other essential parameters such as energy dissipation and stiffness. Especially regarding energy dissipation, wider strips significantly enhanced the ductility and deformation capacity under load by absorbing more energy. This improvement provides notable advantages in strengthening reinforced concrete structures

subjected to repetitive and dynamic loads, such as earthquakes.

In contrast, Sneed et al.[35] previously reported that strip width had limited impact on bond strength in FRCM-type systems. However, the findings of this study partially challenge that view, emphasizing that strip width may indeed be a significantly more critical parameter in TRM systems. These differences could result from various factors, including textile material type, matrix properties, and concrete surface characteristics. Thus, considering the differing findings in existing literature, additional experimental research exploring the influence of strip width under various conditions is necessary.

3.3 | Effect of concrete strength

A detailed evaluation of the experimental findings has demonstrated that concrete compressive strength significantly and critically affects the bond performance at the TRM–concrete interface. Concrete strength emerges as a direct and meaningful parameter when examining the adhesion capacity of TRM systems, maximum load-carrying ability, stiffness, and energy dissipation.

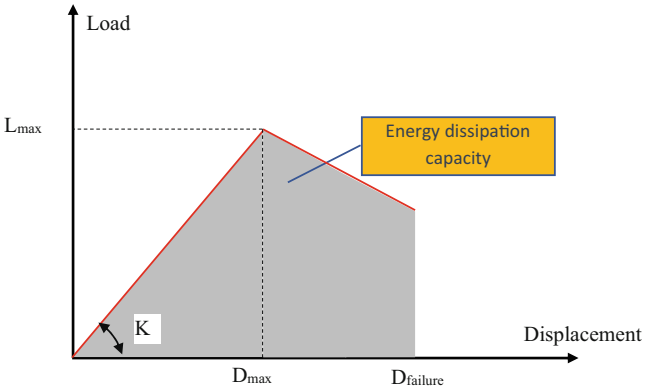

FIGURE 9 Example of performance index calculations.

Increasing concrete compressive strength from 15 to 30 MPa led to notable improvements in maximum load-carrying capacity. For example, in specimens with a strip width of 50 mm and a bond length of 150 mm, an increase in concrete strength resulted in approximately a 30% rise in maximum load capacity, from 4.06 to 5.28 kN. As the bond length increased, the positive effect of concrete strength became even more pronounced, with load capacity increases of 13% at 300 mm (from 7.23 to 8.16 kN) and 23% at 450 mm (from 8.11 to 10.01 kN). For wider strips (100 mm), the effect of concrete strength on load capacity was even stronger, showing increases ranging between 29% and 32%, especially at bond lengths of 300 and 450 mm. This indicates that higher-strength concrete provides a stronger bonding surface, improving stress distribution at the interface and enhancing the load transfer capability from the TRM system to the concrete surface.

The impact of increased concrete strength on stiffness values is also significant. Higher concrete strengths substantially enhanced the stiffness of the TRM–concrete system, reducing deformation under load. For instance, in specimens with a width of 100 mm and a bond length of 300 mm, increasing concrete strength from 15 to 30 MPa approximately doubled stiffness values, rising from 0.70 to 1.42 kN/mm. This suggests that high-strength concrete surfaces allow smaller deformations under load, resulting in more stable and controlled load transfer within the system.

Analyzing the effects of concrete strength on energy dissipation revealed that higher-strength concrete

TABLE 3 Experimental results.

Spec. #	Name	Max load (kN)	Disp. at max load (mm)	Stiffness (kN/mm)	Max. Disp. (mm)	Energy (kN·mm)
1	C15-W50-L150	4.06	7.07	0.57	35.03	63.08
2	C15-W50-L300	7.23	10.32	0.70	20.00	74.58
3	C15-W50-L450	8.11	15.70	0.52	19.82	91.04
4	C15-W100-L150	6.53	11.51	0.57	12.35	38.31
5	C15-W100-L300	9.51	13.54	0.70	31.13	105.74
6	C15-W100-L450	11.17	16.97	0.66	35.98	180.61
7	C30-W50-L150	5.28	6.36	0.83	31.50	72.63
8	C30-W50-L300	8.16	8.90	0.92	54.86	91.99
9	C30-W50-L450	10.01	14.44	0.69	17.49	82.48
10	C30-W100-L150	7.30	9.78	0.75	18.87	64.31
11	C30-W100-L300	12.28	8.65	1.42	27.05	170.67
12	C30-W100-L450	14.78	13.31	1.11	43.24	131.91

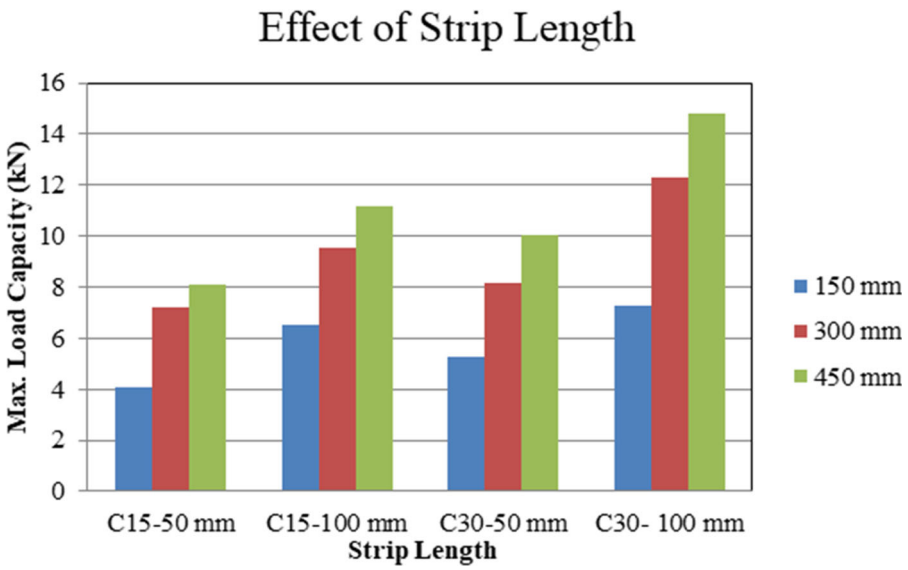

FIGURE 10 Effect of strip length on max. load capacity.

specimens have superior energy absorption capacities. The reason for increased energy absorption is the delayed onset and controlled progression of micro-cracking at the interface region. In particular, for specimens with a width of 100 mm and a bond length of 300 mm, increasing concrete strength from 15 to 30 MPa resulted in a dramatic 61% increase in energy dissipation, from 105.74 to 170.67 kN·mm. This highlights that high-strength concrete surfaces not only facilitate effective load transfer but also absorb greater deformation energy under load, preventing sudden and brittle failures.

Comparison of these results with existing literature confirms the critical role of concrete strength in TRM system performance. D'Antino et al.[32] previously emphasized the direct influence of concrete surface preparation and concrete strength on the adhesion behavior of composite materials, and this study validates the positive contributions of increasing concrete strength to interface performance. Lower bond performance observed in low-strength concretes underscores the importance of surface enhancement and additional preparation procedures before strengthening weak concrete surfaces. Additionally, this highlights the need to consider alternative solutions in designs, such as wider strips or different anchorage methods, when applying TRM systems to weak concrete substrates.

3.4 | Evaluations about stiffness and energy

In addition to maximum load and displacement behaviors, stiffness and energy dissipation properties of TRM–concrete interface systems were comprehensively evaluated in this study. Evaluating these parameters is essential for understanding the structural performance and behavior of TRM strengthening systems. Stiffness is defined as the slope of the linear region in the load–deformation curve, whereas energy dissipation is represented by the area under the load–deformation curve. These two parameters are considered critical indicators, especially regarding the strength, deformation capacity, and post-damage performance of strengthened reinforced concrete structures.

Experimental results revealed a direct correlation between stiffness and parameters such as TRM strip width, bond length, and concrete strength. Generally, increases in concrete strength and strip width significantly improved stiffness. For example, increasing concrete strength from 15 to 30 MPa for specimens with 50 mm strip width and 300 mm bond length resulted in approximately a 31% increase in stiffness, from 0.70 to 0.92 kN/mm. For specimens with 100 mm strip width at the same bond length, this increase in concrete strength resulted in a dramatic doubling of stiffness, approximately a 103% increase, from 0.70 to 1.42 kN/mm. These findings clearly indicate that higher-strength concrete surfaces create a stronger and stiffer connection with TRM strips, resulting in a more rigid system with reduced deformation.

It was observed that as strip width increased, stress distribution within the bond area became more homogeneous, enhancing overall system stiffness. Particularly, for concrete strength of 30 MPa and bond length of 300 mm, increasing the strip width from 50 to 100 mm increased stiffness by 54%, from 0.92 to 1.42 kN/mm. This demonstrates that wider strips exhibit more stable behavior under load, limiting deformations and positively influencing structural performance.

On the other hand, analyzing the effect of bond length on stiffness revealed a relative decrease in stiffness at longer bond lengths. This occurs because deformation spreads over a larger area in longer bond lengths, leading to some loss in stiffness. However, given the corresponding increase in load capacity, this stiffness reduction does

not negatively impact structural performance; instead, it contributes to more ductile behavior.

Energy dissipation was assessed as a critical parameter for understanding the ductility and damage resistance of the bond mechanism. Overall, energy dissipation notably increased with bond length, strip width, and concrete strength. Increased energy dissipation means materials can absorb more deformation energy under load, thereby avoiding brittle failures.

For instance, for low-strength concrete (15 MPa), energy dissipation for specimens with 100 mm width and 150 mm bond length was 38.31 kN·mm, increasing nearly fivefold to 180.61 kN·mm when bond length was extended to 450 mm. When concrete strength increased (30 MPa), for the same strip width and a bond length of 300 mm, energy dissipation rose by 61%, from 105.74 to 170.67 kN·mm. This indicates that higher-strength concrete surfaces better control stresses and deformations in the bond region, delaying crack progression and allowing the system to absorb more energy.

3.5 | General evaluations and discussions

The results obtained from this experimental study provide critical insights into the bond behavior of TRM strips to concrete surfaces. Compared to the existing literature, the findings both confirm some significant previous results and reveal effects of parameters that have either been minimally investigated or not addressed at all.

Firstly, a notable increase in maximum load capacity was observed with an increase in bond length, aligning with similar results reported by D'Antino et al.[33] and Tran et al.[35] However, it was observed that extending the bond length beyond a certain threshold (e.g., beyond 300 mm) led to limited additional gains in load capacity. This finding supports the concept of an effective bond length for TRM strips and highlights the necessity of determining critical threshold values in design.

Another notable point is the relationship between maximum displacement values and energy dissipation. Generally, maximum displacements tend to be higher in longer bond lengths and wider strips, directly contributing to increased energy dissipation. Particularly, specimens with 30 MPa concrete strength showed higher maximum displacements and consequently higher energy dissipation, clearly emphasizing the importance of concrete strength and TRM geometry on energy absorption capacity.

The impact of strip width on bond performance is one of the most original findings of this study. The experiments demonstrated that increasing the TRM strip width significantly enhanced load-carrying capacity, particularly

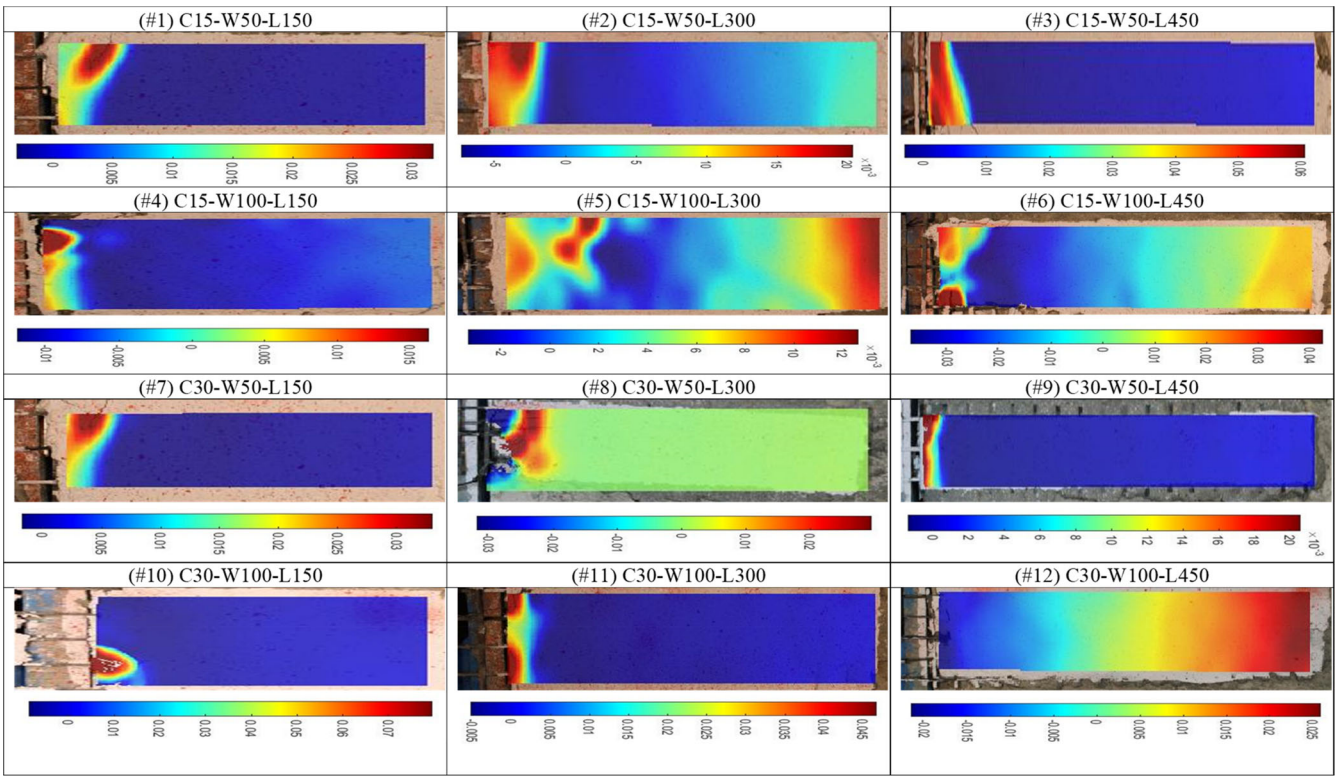

FIGURE 11 Strain distribution on x-axis with original legend ($\mathcal{E}_{xx}$).[44]

at larger bond lengths. This indicates that the often-neglected strip width parameter is, in fact, an essential design parameter and must be considered carefully in strengthening applications.

Increasing concrete compressive strength notably improved bond performance, leading to significant enhancements in parameters such as maximum load capacity, stiffness, and energy dissipation. The low bond performance observed in lower-strength concrete highlights the necessity for surface enhancement prior to strengthening applications and suggests that concrete strength should be a central consideration when determining strengthening strategies for existing concrete structures.

Evaluating stiffness and energy dissipation results provides significant insights into the structural performance of the TRM–concrete system. The observed increase in stiffness, particularly with higher concrete strength and wider TRM strips, offers advantages in reducing deformations induced by applied loads. This positively impacts the service life and serviceability limit states of strengthened structures. Additionally, substantial increases in energy dissipation demonstrate that extending TRM bond length and increasing strip width significantly enhance system ductility and energy absorption capacity. These findings indicate that TRM–strengthened concrete structures may exhibit considerable performance advantages under dynamic loading conditions such as earthquakes.

The outcomes of this study hold considerable importance for improving existing TRM design models. Specifically, effectively utilizing parameters such as bond length and strip width can refine and economize design standards. The insufficient representation of these parameters in current design guidelines prevents optimal use of TRM systems, leading to increased strengthening costs and potential underperformance concerning desired objectives.

Future research should explore additional parameters, including various types of TRM (e.g., glass and basalt fiber TRM), different mortar types, diverse concrete classes, and surface treatments. Moreover, investigating loading rates and environmental conditions (such as high temperatures, moisture, and freeze–thaw cycles) on bond behavior warrants separate attention. Evaluating bond strength under prolonged loading and fatigue effects is also crucial for assessing the long-term performance of TRM systems.

In conclusion, the findings obtained provide critical insights into key design parameters for more effective and economical use of TRM systems in strengthening projects, contributing original and valuable perspectives to existing literature. Future studies that expand on these results with more comprehensive analyses are expected to further enhance the application of TRM systems in reinforcing concrete structures.

3.6 | Results of DIC measurements

The strain distributions (Ɛxx) on the surfaces of the test specimens were analyzed in two distinct ways. Initially, strain distributions were determined individually for each specimen using their original legends. Subsequently, strain distributions were re-assessed for all specimens based on a common legend. Strain distributions according to both original and common legends are presented in Figures 11 and 12, respectively. Additionally, damage distributions observed on specimens' post-experiment are depicted in Figure 13. The impacts of concrete grade (C15–C30), TRM strip width (50–100 mm), and TRM strip length (150–300–450 mm) on the results obtained from DIC analysis were compared. According to the DIC results, areas of maximum strain concentration varied depending on concrete grade, TRM strip width, and length, typically concentrating near the edge closest to the hydraulic loading system, while significantly lower strain variations were observed at the center and at the farthest edges from the loading point. The following conclusions were derived regarding strain values:

- Examining strain values with respect to concrete grade (C15, C30), maximum strain values were recorded for specimens numbered 1, 3, and 6 (C15 concrete), and specimens numbered 8, 10, and 11 (C30 concrete). It was concluded that the average strain values obtained from C30 concrete specimens were higher than those from C15 concrete specimens.
- Investigating the influence of TRM strip width (50–100 mm) on strain values, maximum strains were recorded in specimens numbered 1, 3, 7, and 8 with 50 mm TRM strip widths, and in specimens numbered 6, 10, and 11 with 100 mm TRM strip widths. However, the average strain value for specimens with 50 mm TRM strips was slightly higher compared to those with 100 mm TRM strips.
- When examining strain values based on TRM strip length (150–300–450 mm), maximum strains were noted in specimens numbered 7 and 10 with 150 mm strip lengths, specimens numbered 8 and 11 with 300 mm strip lengths, and specimens numbered 3 and 6 with 450 mm strip lengths. It was determined that the average strain values increased with the length of the TRM strips, with specimens featuring 450 mm strip lengths exhibiting higher average strains compared to those with 300 and 150 mm lengths.

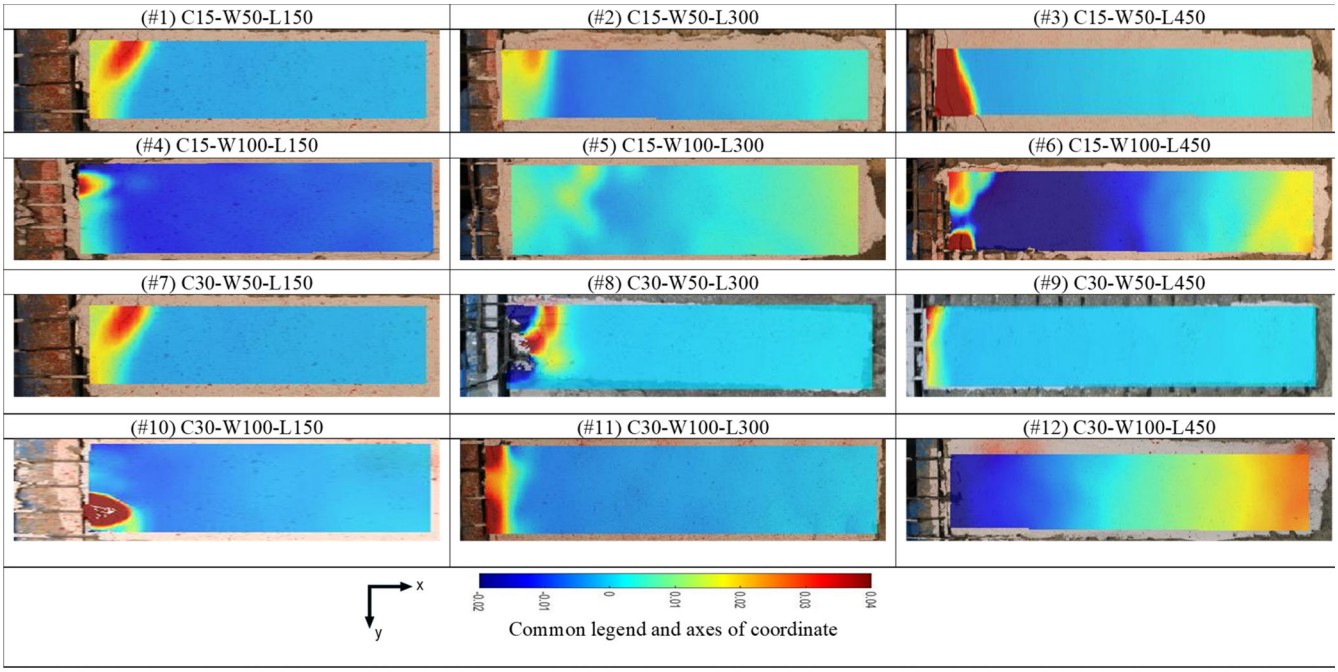

FIGURE 12 Stress distribution on *x*-axis with common legend ($\mathcal{E}_{xx}$).[44]

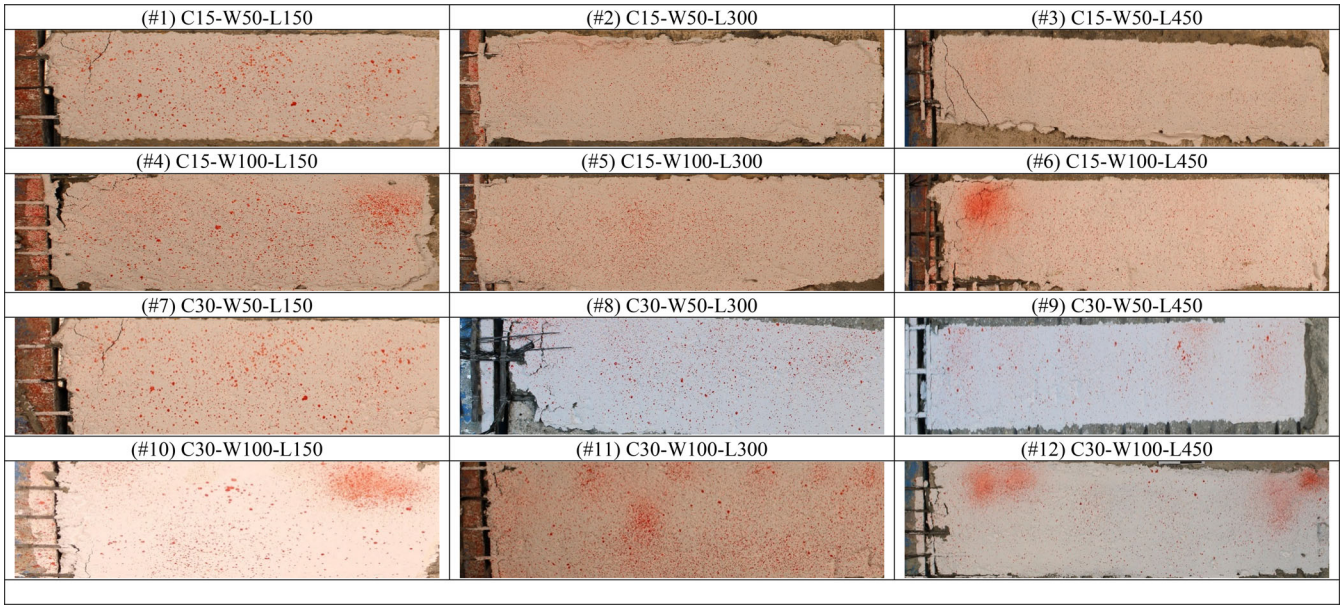

FIGURE 13 Failure modes of the specimens.[44]

4 | PROPOSED MODELS

Accurately defining the interaction between the TRM and the concrete substrate is of critical importance in the numerical analysis of TRM-strengthened reinforced concrete elements. In the ABAQUS finite element software, surface-based cohesive zone models (CZM) are commonly employed, utilizing the traction–separation law illustrated in Figure 14. To implement this type of surface-based cohesive zone model at the interface, three fundamental parameters are typically required: the maximum shear stress, the stiffness, or the displacement at maximum load, and the fracture energy, which corresponds to the area under the shear stress–displacement curve. Using these three parameters, the backbone curve of the interface behavior can be effectively represented.

In order to characterize the interface behavior within the scope of the present experimental study, a linear/

nonlinear regression analysis was conducted in Microsoft Excel based on the experimental findings. It should be noted that the following equations are empirical relationships derived from a limited experimental database and are not intended to represent generalized predictive models. It should be emphasized that the proposed regression equations are not intended to function as standalone design or reference equations, but rather as auxiliary formulations to define the cohesive zone model parameters within the numerical framework of the present study. As a result of this regression study, four equations were proposed to describe the bond–slip behavior at the TRM–concrete interface for the investigated parameter range, considering the compressive strength of the concrete, TRM strip width, and TRM bonding length as independent variables. The maximum load corresponding to the debonding of the strips from the surface can be estimated using Equation (1). The displacement value at the maximum load or maximum shear stress can be calculated using Equation (2). Furthermore, the maximum interface shear stress to be used in both the backbone curve and the CZM model can be determined using Equation (3). Finally, the total area under the stress–displacement curve, representing the

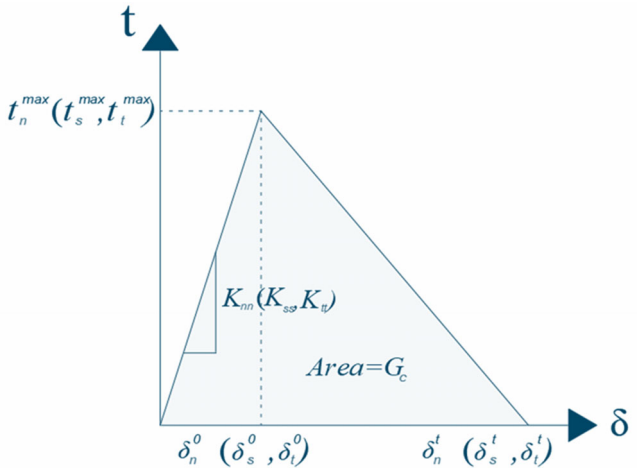

FIGURE 14 Traction–separation curves for the cohesive zone model.

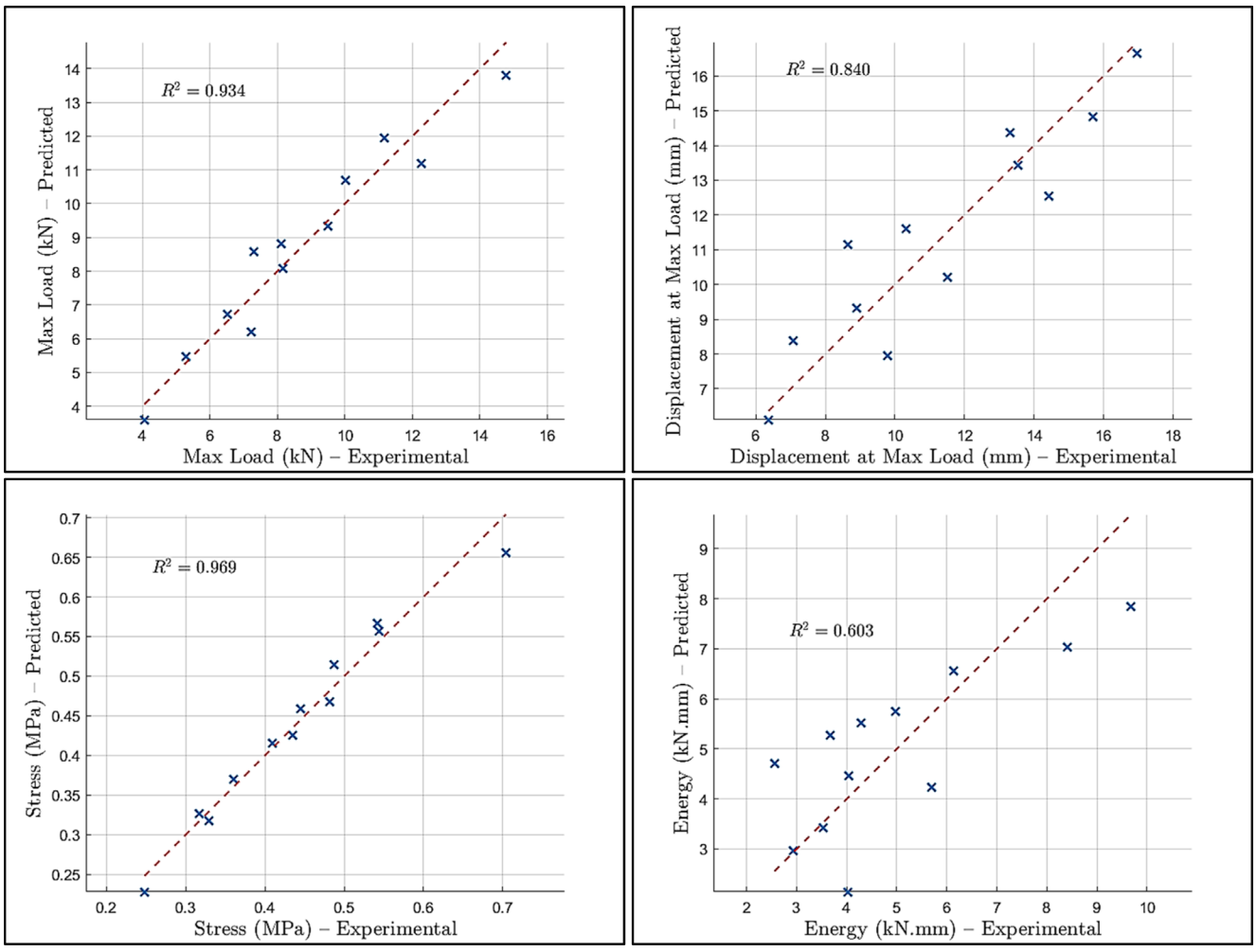

FIGURE 15 Accuracy of prediction models based on experimental data (max load, displacement at max load, stress, energy).

TABLE 4 Summary of p-values for model predictors.

Model	Intercept	C (concrete)	W (strip width)	L (bonding length)
Max load	0.0163	0.0077	0.0004	0.0000
Displacement	0.0411	0.0393	0.0838	0.0005
Stress	0.0000	0.0003	0.0000	0.0000
Energy	0.0028	0.4070	0.0369	0.0535

fracture energy, is computed using Equation (4), noting that further experimental testing with a larger number of specimens and detailed statistical analysis would be required to develop more robust and widely applicable predictive models.

$$F_{\max}\,(\mathrm{kN}) = -4.003 + 0.124 \cdot C + 0.0624 \cdot W + 0.0174 \cdot L \tag{1}$$

$$\Delta_{\max-\mathrm{load}}\,(\mathrm{mm}) = 5.629 - 0.152 \cdot C + 0.0366 \cdot W + 0.0214 \cdot L \tag{2}$$

$$\tau_{\max}\,(\mathrm{MPa}) = 0.718 + 0.00593 \cdot C - 0.00284 \cdot W - 0.00065 \cdot L \tag{3}$$

$$G_{\mathrm{total-energy}}(\mathrm{N/mm}) = 9.823 + 0.0541 \cdot C - 0.0464 \cdot W - 0.00857 \cdot L \tag{4}$$

The predictive performance of the four regression equations proposed through the regression analysis is illustrated in the graphs provided in Figure 15, where the calculated determination coefficients (R^2) for each model are also indicated. Table 4 presents the p-values of the independent variables used in the regression models developed for estimating the maximum load, displacement at maximum load, bond stress, and energy absorption capacity. The p-value is a statistical measure that indicates whether an independent variable has a significant effect on the regression model; typically, a value of $p < 0.05$ implies that the variable contributes significantly to the model. According to the results, all input variables concrete compressive strength (C), TRM strip width (W), and bonding length (L) were found to be statistically significant ($p < 0.05$) in the Maximum Load and Bond Stress models. This suggests that these three parameters have a strong influence on the corresponding model outputs. In the Displacement at Maximum Load model, bonding length emerged as a highly significant parameter ($p = 0.0005$), while strip width was marginally significant ($p = 0.0838$), and concrete grade was also statistically significant ($p = 0.0393$). On the other hand, in the Energy model, only the strip width was found to be significant ($p = 0.0369$), whereas the contributions of concrete grade and bonding length were not statistically meaningful. These findings indicate that while some parameters consistently and strongly influence structural performance, others may exhibit limited or response-dependent effects.

Figure 16 presents the backbone curves generated using the proposed bond-slip equations for both C15 and C30 concrete grades. Each curve follows a simplified triangular shape defined by the predicted bond stress and the displacement at maximum load. To ensure that the model reflects the actual energy dissipation, the maximum displacement was not taken directly from the experiments. Instead, it was calculated so that the area under the triangle equals the total energy predicted by the regression model. This way, a more consistent and physically meaningful representation of the interface behavior was achieved.

5 | NUMERICAL ANALYSIS

In the numerical analysis part of the study, the experimental work conducted by Tetta et al.[48] was taken as a basis in order to validate the proposed numerical modeling approach and to establish a direct link with experimentally observed TRM-to-concrete bond behavior. The study by Tetta et al. was selected due to its strong relevance to the present work, as it investigates TRM-to-concrete interfaces without mechanical anchorage under comparable material configurations and loading conditions. Accordingly, the geometric dimensions, material properties, longitudinal and transverse reinforcement layout, and TRM strengthening details of the RC beam specimens were modeled exactly as in the original experimental program using the Abaqus finite element analysis software.[49] Abaqus is a strong solver known for its extensive material library as well as analysis characteristics and its ability to provide reliable results under various loading conditions. For this reason, it is frequently used by researchers to validate experimental results and obtain the behavior of test specimens in the computer environment.[50–52] In addition, the software offers various solution technologies to perform linear and non-linear analyses with several modules that can work together.

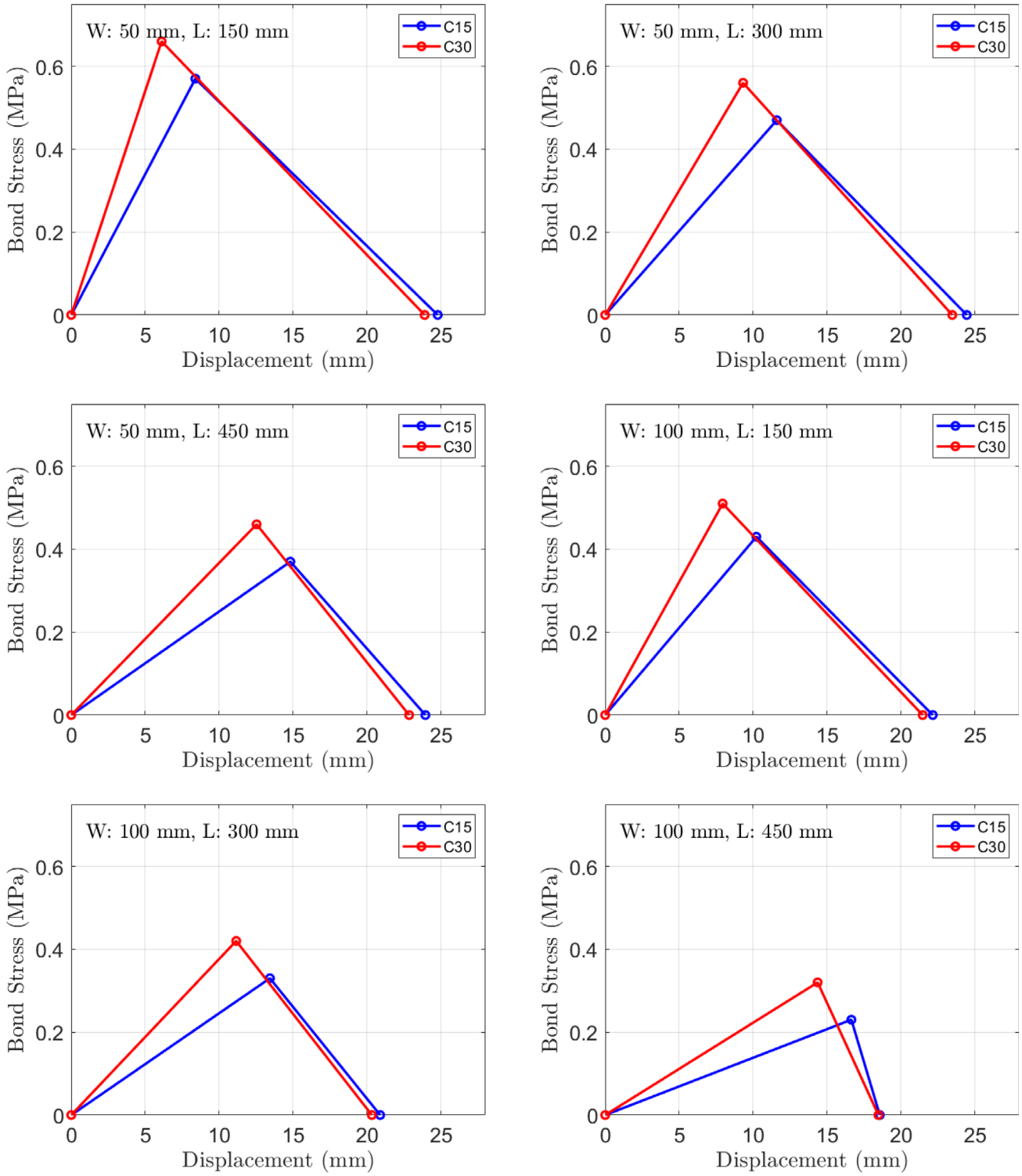

FIGURE 16 Backbone curves based on proposed bond-slip equations for C15 and C30 concrete.

The finite element models of the specimens were constituted in the first step of the numerical analysis. Three-dimensional 8-node linear brick, hexahedron element type (C3D8R) elements were used to model three-dimensional models of the concrete beams and TRM strips in the software. On the other hand, two-node beam elements (B31) were utilized in modeling the longitudinal and transverse steel reinforcement. To provide the interaction between the concrete and the reinforcement, the embedded region constraint property of Abaqus is used. These element types are exhibited in Figure 17.

The geometric dimensions and the reinforcement configuration of the specimens were taken to be the same

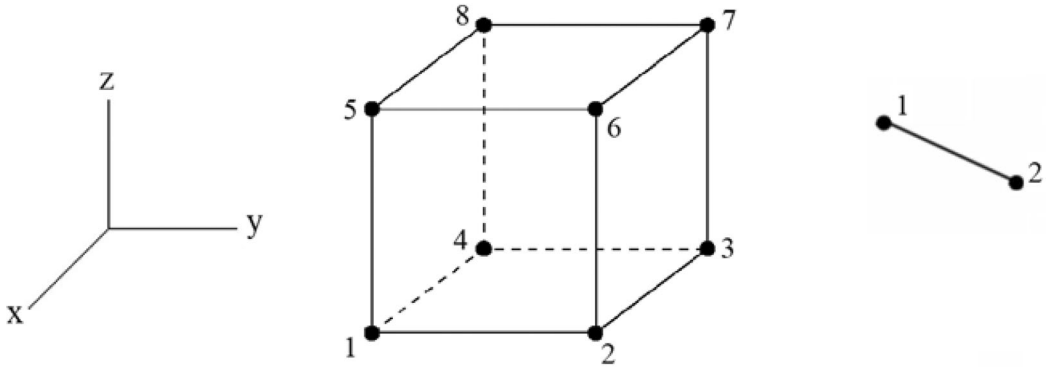

FIGURE 17 The element types.

as the experimental study. RC beams having 102 × 203 mm section sizes with 26 mm concrete cover were intentionally designed to exhibit shear deficiency within one of the two shear spans to replicate the traditional detailing practices. Specifically, the critical shorter shear span, measuring 460 mm in length, was considered without any stirrups. In contrast, the longer shear span was reinforced with 8 mm diameter stirrups 75 mm apart. Besides, two 16 mm-diameter longitudinal steel bars were placed in the tension zone, and two 10 mm-diameter bars were placed in the compression zone of the rectangular sectioned RC beams. The reinforcement details of the specimens are presented in Figure 18.

TRM strengthening was applied at the critical shear span of the RC beams to improve their shear resistance in the experimental program.[48] In addition, the number of layers and configuration of TRM strips are the other investigated parameters. The specimens were strengthened by three different configurations such as side-bonded, u-wrapped, and fully wrapped TRM strips. Besides, 1–3 TRM layers were applied on the RC beams in the strengthening procedure, allowing for a consistent comparison between experimental observations and numerical predictions. Properties of the specimens due to TRM strengthening are detailed in Table 5.

All of the specimens with different strengthening configurations were modeled in the software. Afterwards, material properties of concrete obtained in the experimental study were defined via concrete damage plasticity (CDP) model existing in the material library of the software. CDP model which is a continuum, plasticity-based, damage material model enables users to model the complex behavior of concrete both in compression and tension parts. As compression strength values of the specimens are 21.6, 22.6 and 23.8 MPa in the experimental study, three concrete models are defined in the software.

The uniaxial compressive and tensile behaviors of concrete are represented using the CDP model. In

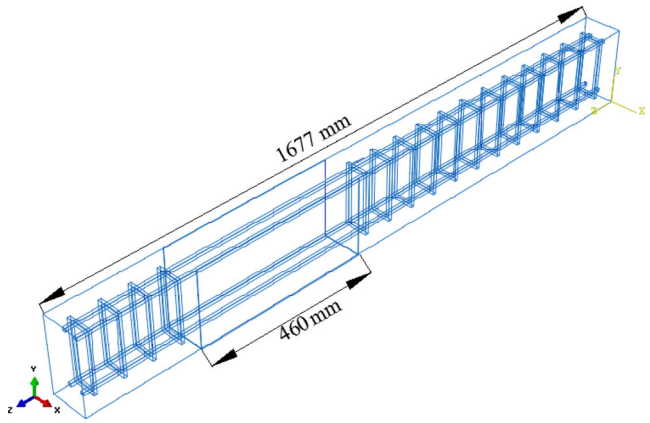

FIGURE 18 Reinforcement details.

TABLE 5 Properties of the specimens.

Specimen	TRM configuration	Number of layers
S1	Side-bonded	1
S2	Side-bonded	2
S3	Side-bonded	3
S4	U-wrapped	1
S5	U-wrapped	2
S6	U-wrapped	3
S7	Fully-wrapped	1
S8	Fully-wrapped	2

uniaxial compression, the response follows a linear path up to the initial yield stress (σ_{c0}). Beyond this point, the behavior transitions into a nonlinear regime characterized by stress hardening, followed by strain softening beyond the ultimate compressive strength (σ_{cu}), within the plastic deformation zone. In the uniaxial tension region, the material exhibits a linear elastic response up to the tensile failure stress (σ_{t0}), which marks the initiation of microcracking in the concrete matrix. Beyond this stress level, a strain-softening behavior governs the

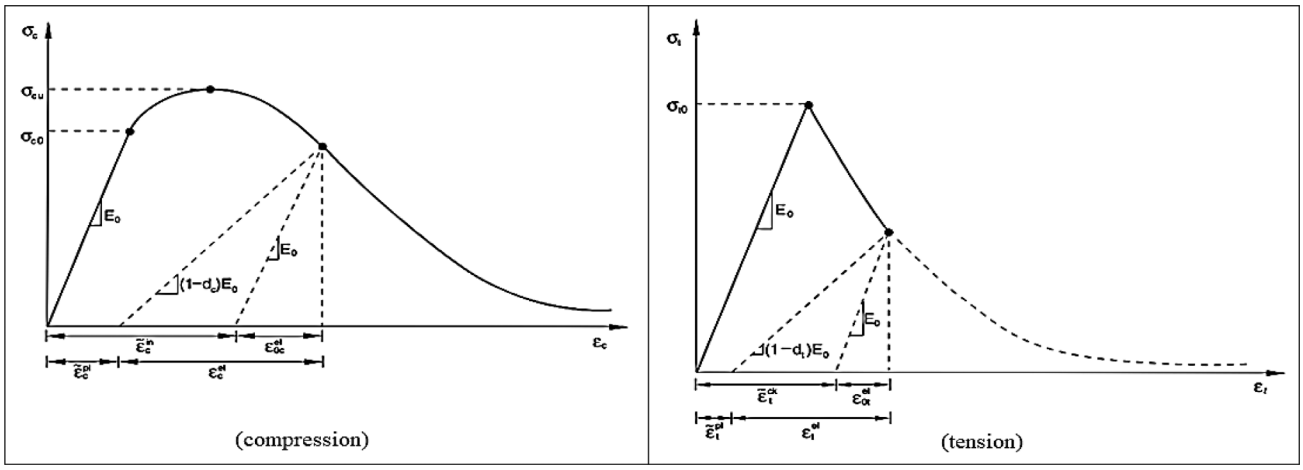

FIGURE 19 Stress–strain curves of concrete.

TABLE 6 Material characteristics of concrete.

Property	Values for S1, S7, S8	Values for S2, S3, S6	Values for S4, S5
Poisson's ratio	0.20		
Density (kg/m^3)	2400		
Modulus of elasticity (MPa)	21843.6	22343.5	22929.1
Compressive strength (MPa)	21.6	22.6	23.8
Tensile strength (MPa)	2.89	2.96	3.04
ψ	30		
e	0.10		
σ_{b0}/σ_{c0}	1.16		
K_c	0.6667		
μ	0.0001		

response, reflecting the progressive development of micro-cracks. The stress–strain relationships for both compression and tension are illustrated in Figure 19.

In the CDP model, two damage variables, denoted as d_t and d_c, are employed to represent the degradation of elastic stiffness under tensile and compressive loading, respectively. These variables range from 0 to 1, where a value of 0 indicates an undamaged state and a value of 1 corresponds to complete loss of load-carrying capacity. The stress–strain responses under tension and compression are formulated using these damage parameters. In the corresponding equations, E_0 denotes the initial elastic modulus of the material, while $\tilde{\varepsilon}_t^{pl}$, and $\tilde{\varepsilon}_c^{pl}$, represent the equivalent plastic strains in tension and compression, respectively.

$$\sigma_t = (1-d_t)E_0\left(\varepsilon_t - \tilde{\varepsilon}_t^{pl}\right) \quad (5)$$

$$\sigma_c = (1-d_c)E_0\left(\varepsilon_c - \tilde{\varepsilon}_c^{pl}\right) \quad (6)$$

For a clearer representation of the damage variables, Equations (5) and (6) can be reformulated as shown below. The equivalent plastic strains, $\tilde{\varepsilon}_t^{pl} = b_t\tilde{\varepsilon}_t^{ck}$ and $\tilde{\varepsilon}_c^{pl} = b_c\tilde{\varepsilon}_c^{ck}$, appear in Equations (7) and (8). The parameters b_t and b_c are recommended as 0.1 and 0.7, respectively, based on the findings of Birtel and Mark.[53] Additional plasticity parameters in the CDP model include the dilation angle (ψ), flow potential eccentricity (e), the ratio of initial equibiaxial compressive yield stress to initial uniaxial compressive yield stress (σ_{bo}/σ_{co}), the coefficient defining the shape of the deviatoric cross-section (K), and the viscosity parameter (μ). These parameters are essential for defining the yield surface, the flow potential, and the viscous behavior of concrete.

$$d_t = 1 - \frac{\sigma_t/E_0}{\tilde{\varepsilon}_t^{pl}\left(\frac{1}{b_t}-1\right)+\sigma_t/E_0} \quad (7)$$

$$d_c = 1 - \frac{\sigma_c/E_0}{\tilde{\varepsilon}_c^{pl}\left(\frac{1}{b_c}-1\right)+\sigma_c/E_0} \quad (8)$$

The compressive behavior of unconfined concrete was defined using the stress–strain relationship proposed by Mander et al.[54] In this model, the ultimate compressive strain of concrete (ε_{cu}) was assumed to be 0.003. For the tensile behavior, the ultimate tensile strain (ε_{tu}) was defined as $\varepsilon_{tu} = 10\varepsilon_{cr}$ where ε_{cr} denotes the strain corresponding to the peak tensile strength. The tensile response was idealized as linearly increasing up to (ε_{cr}), followed by a linear softening phase extending to (ε_{tu}).

The elastic modulus of concrete (E_c) was calculated based on its compressive strength (f_c) using Equation (9). Similarly, the tensile strength of concrete (f_t) was estimated by Equation (10), as proposed by Obeidat et al.[55] and Li et al.[56] The values of Poisson's ratio and density were taken as 0.2 and 2400 kg/m^3, respectively. The material properties of concrete, including the plasticity parameters used for numerical modeling, are summarized in Table 6.

$$E_c = 4700\sqrt{f_c} \tag{9}$$

$$f_t = 0.623\sqrt{f_c} \tag{10}$$

The material properties of the steel reinforcement and loading plate were also defined within the numerical model. The interaction between the concrete and the steel reinforcement was ensured using the embedded

TABLE 7 Material characteristics of steel.

Property	Value
Poisson's ratio	0.30
Density (kg/m^3)	7850
Young's modulus (MPa)	200,000
Shear modulus (MPa)	76923.08
Bulk modulus (MPa)	166666.67

TABLE 8 Number of nodes and elements.

Specimen	Number of nodes	Number of elements
S1	26,452	17,091
S2	26,717	17,432
S3	27,518	18,303
S4	26,836	17,367
S5	27,641	17,714
S6	28,470	18,069
S7	27,321	17,723
S8	27,949	18,548

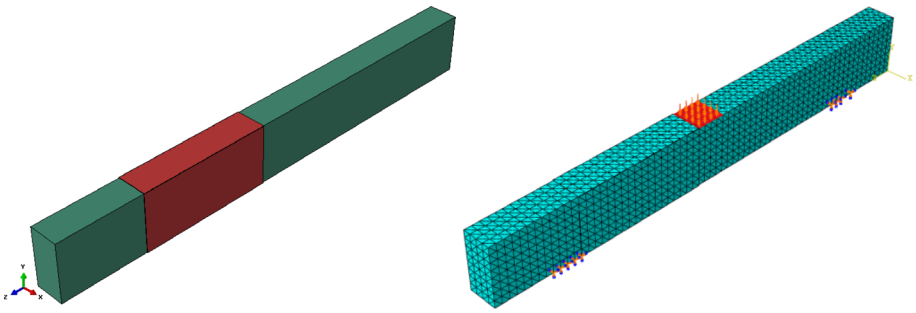

FIGURE 20 Specimen-7 after mesh design.

TABLE 9 Comparison of experimental and numerical results.

	Ultimate load capacity			Displacement at ultimate load		
Specimen	Experimental	Numerical	Ratio	Experimental	Numerical	Ratio
S1	56.6	62.4	0.91	2.2	2.7	0.81
S2	88.7	93.6	0.95	4.7	5.4	0.87
S3	108.9	103.2	1.06	5	5.8	0.86
S4	78.2	75.3	1.04	3	3.6	0.83
S5	120.2	129.5	0.93	5.4	6.2	0.87
S6	131.1	144.6	0.91	5.5	5.9	0.93
S7	111.2	120.3	0.92	6	7.1	0.85
S8	152.8	165.2	0.92	6.1	7.5	0.81
Average			0.95			0.86

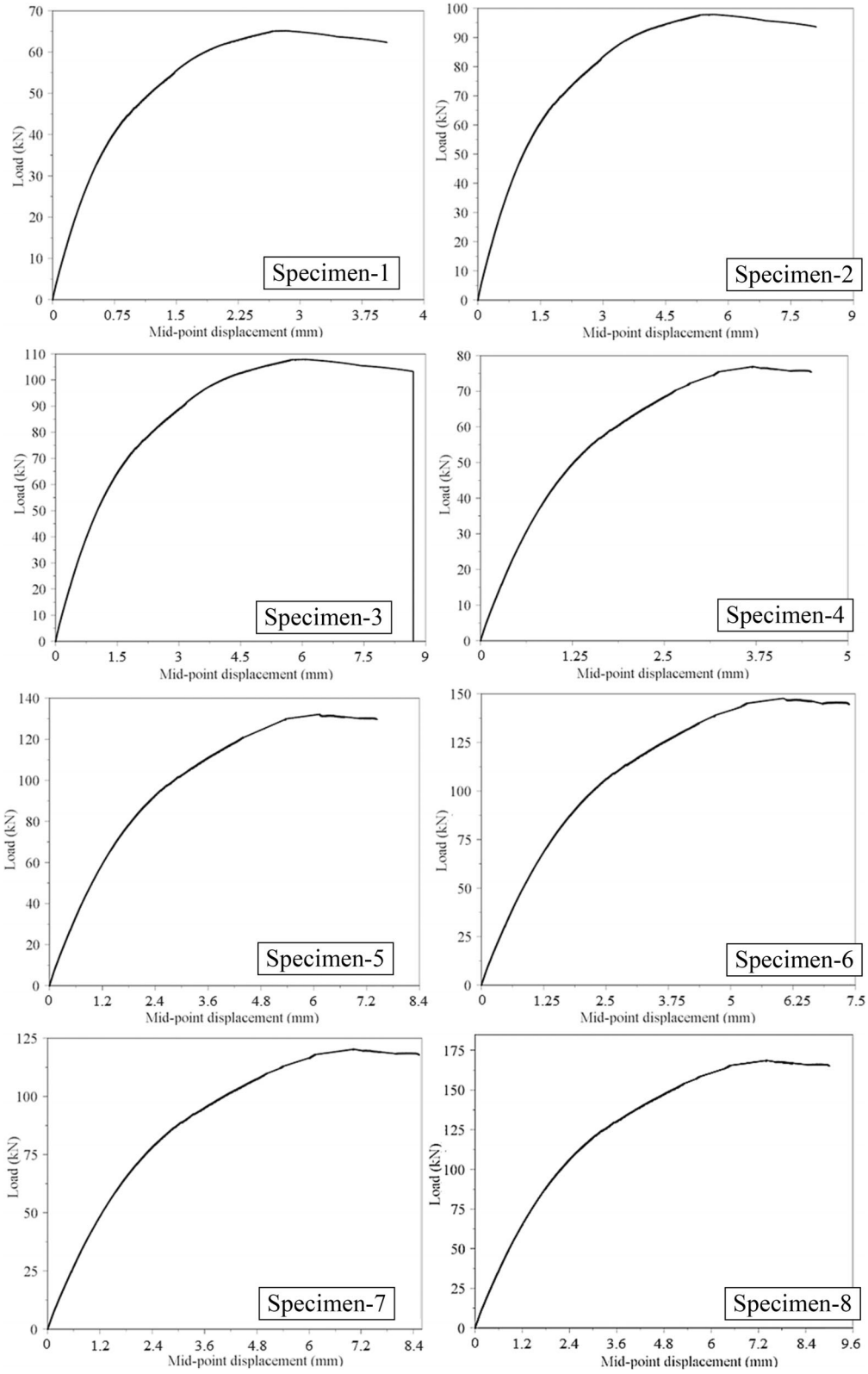

FIGURE 21 Load–displacement curves.

region constraint feature available in Abaqus, thereby ensuring perfect bond between the two materials. The steel reinforcement was modeled as an elastoplastic material without hardening, whereas a linear elastic material model was employed for both the loading plate and the impact hammer. In the experimental study, the yield strength of the 10- and 16-mm diameter longitudinal bars were determined as 547 and 552 MPa, respectively while the strength of the 8-mm diameter bars used for stirrups was 568 MPa. In addition, the values of

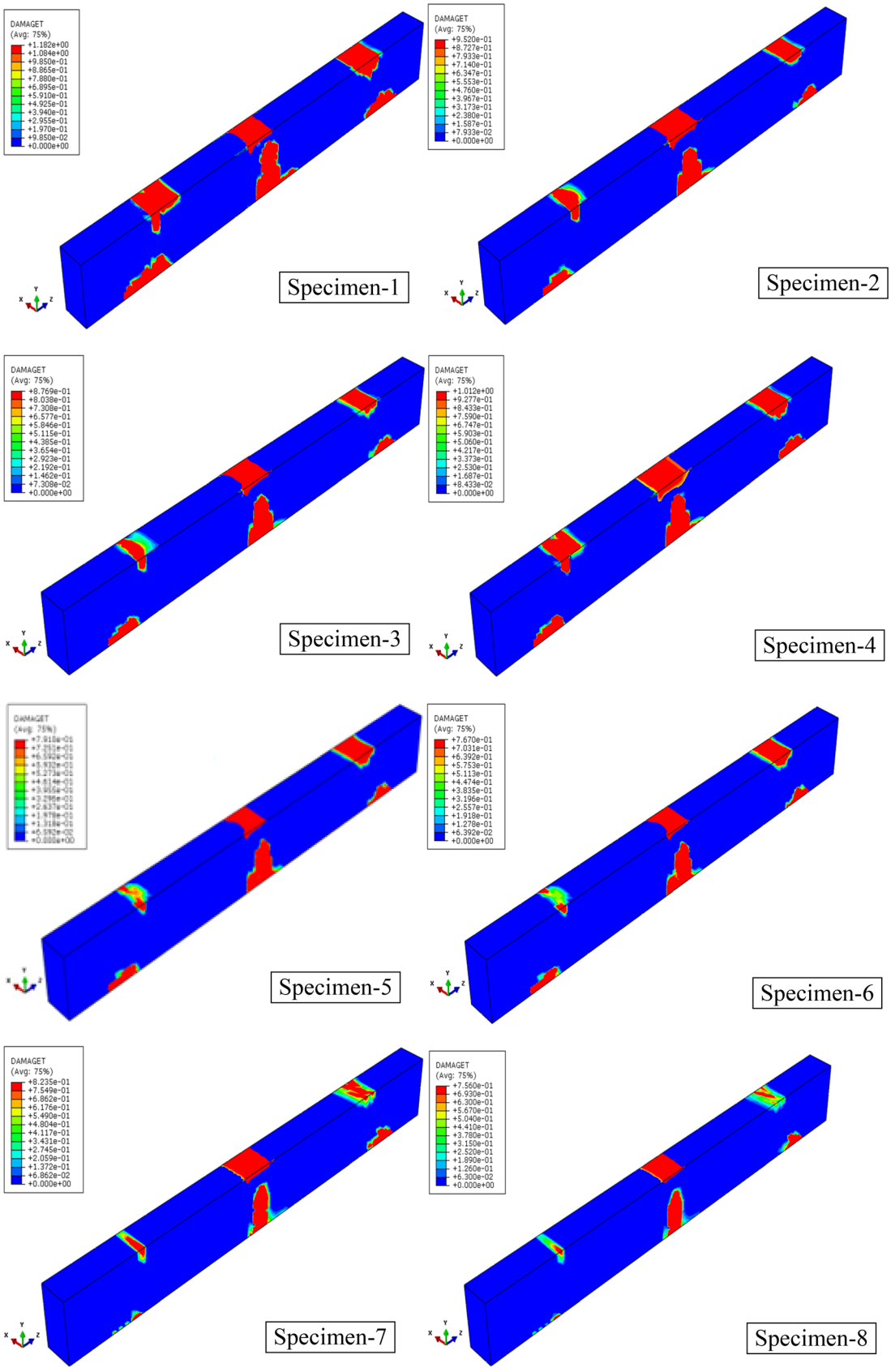

FIGURE 22 Crack formations.

Poisson's ratio, Young's modulus, bulk modulus, and shear modulus for the steel material are presented in Table 7.

TRM strips with different configurations were applied in the related directions as strengthening materials on RC beams. To ensure an ideal bond without any separation between the TRM strips and the specimens, a perfect interface condition was assumed in the numerical model. In the case of three-layer TRM configurations, each TRM layer was modeled explicitly, and a perfect bond assumption was adopted between adjacent TRM layers. Accordingly, no relative slip or separation was allowed between the TRM layers, representing the monolithic behavior of the composite system observed in the experimental tests.

The proposed material model in Figure 14 was adopted in the numerical analysis via the cohesive zone model (CZM) feature of the software. Accordingly, the TRM strips were modeled as elastic materials using fully integrated elements. The characteristics of the TRM strips were taken from the experimental study assigned to the respective sections. The tensile strength and the elastic modulus were taken as 3800 MPa and 225 GPa, respectively. Besides, the thickness of mortar was taken as 2 mm. Textile meshes were embedded in the TRM strips in the finite element models. The cohesive traction–separation law shown in Figure 14 was employed exclusively to simulate the bond behavior at the TRM–concrete interface. Additionally, surface-based tie constraints were employed to define the interaction between the inner surface of the TRM strips and the concrete surface of the strengthened RC beams. In this constraint definition, the concrete surface was designated as the master surface, while the inner surface of the TRM strip was assigned as the slave surface.

Finite element models were separated into smaller parts to obtain more accurate results. For this purpose, a mesh convergence study was performed for Specimen 1 to decide the optimum finite element size. The numerical analysis was repeated for different values between 10 and 40 mm. No remarkable changes were obtained for the values smaller than 25 mm. However, it was found that further decreases in the mesh size extended solution time. So, the finite element size was decided as 25 mm for all specimens. Based on the determined mesh size values, the number of elements and nodes for all components was obtained. The values are given for each specimen in Table 8. Besides, the finite element model of Specimen 7 is shown before and after the mesh design in Figure 20.

Time interval (Δt) is another significant parameter in numerical analysis. This value is considered as 0.01 s in the software. Afterwards, RC beams were subjected to three-point bending due to the changes in TRM configurations. Numerical analysis was performed to the failure damage situation. So, load and displacement values were obtained for each specimen in the end. The values are comparatively presented in Table 9. In addition, load–midpoint displacement curves were also determined after numerical analysis in the software. These curves are exhibited in Figure 21. When the relationship between experimental and numerical values is evaluated, it is seen that a strong relationship is established between both results. So, it is thought that the proposed numerical model could be useful in the verification of experimental results in future studies.

In the last step of the numerical analysis, crack distributions were obtained from the software under three-point bending. For this purpose, the damage function of the software was utilized. Damage distributions of the specimens are presented in Figure 22. It is seen that fractures are generally accumulated around the loading point and expand to the supports. Besides, the effect of strengthening on crack formations is observed due to the varied configurations and layers of TRM strips. Similar to the experimental study, as the number of strengthened sides and the number of layers to which TRM strengthening was applied in the specimens increased, a decrease in the damage distributions was observed.

6 | CONCLUSIONS

This comprehensive experimental investigation focused on assessing the bond–slip behavior between TRM composites and concrete substrates, highlighting several key parameters: concrete compressive strength, TRM strip width, and bonding length that significantly influence structural performance. Based on the results obtained from 12 designed specimens, the following conclusions can be drawn:

- Increasing the bonding length significantly enhanced the maximum load-carrying capacity of the TRM–concrete interface. However, the effectiveness of increased bonding length became limited beyond 300 mm, indicating an effective anchorage length threshold.
- The increase in TRM strip width from 50 to 100 mm notably improved both the load-carrying capacity and energy absorption capability. The wider strips facilitated better distribution of stresses along the interface, reducing localized stress concentrations.
- Increasing concrete compressive strength from 15 to 30 MPa substantially improved bond performance, stiffness, and energy absorption capacity. Higher-strength concrete substrates provided a more robust

bonding interface, enabling more effective load transfer and increased resilience against deformation and sudden failures.

- Increasing the TRM strip width and bonded length consistently improved structural performance, although the effect of bonded length showed signs of plateauing beyond 300 mm. Higher concrete compressive strength also contributed to improved bond performance, particularly when combined with wide strips.
- Digital Image Correlation analyses effectively demonstrated localized strain distributions, highlighting the critical zones prone to interface failure. Specimens with higher concrete grades exhibited greater average strain values, while increased strip width slightly reduced localized strain concentrations. Longer strips uniformly distributed strain over a broader region, improving overall structural ductility and energy dissipation characteristics.
- Regression analyses facilitated the development of robust predictive equations for key interface parameters: maximum load, displacement at maximum load, bond stress, and energy absorption. These predictive models, incorporating concrete compressive strength, TRM strip width, and bonding length, showed high accuracy and statistical significance, providing valuable tools for engineers to optimize and accurately model TRM-strengthened concrete structures in numerical analyses.

The experimental investigation is limited to 12 single-lap bond specimens covering a specific range of parameters, including two concrete strength classes, two strip widths, and three bond lengths, and focuses on a single TRM system with unanchored configurations under quasi-static loading. Accordingly, the observed trends represent the monotonic bond–slip response and do not explicitly account for cyclic loading, rate effects, environmental conditions, or alternative textile–mortar systems. The regression-based equations proposed in this study were calibrated using the present experimental dataset and employed to define interface parameters within the numerical framework; additional experimental data would be beneficial to further assess their robustness and extend their applicability.

Further research should expand to include additional parameters such as different textile materials (e.g., glass, basalt), varying mortar compositions, diverse environmental conditions, usage anchor, and long-term load effects. Understanding the impact of these additional factors would further refine the design guidelines for TRM systems, enhancing their practical applicability and structural reliability.

In conclusion, this study significantly advances the understanding of the complex interaction between TRM composites and concrete substrates, fills critical gaps in existing literature, and provides essential insights and analytical tools for the optimized design and application of TRM strengthening techniques in concrete structures.

ACKNOWLEDGMENTS

This study was supported by the Scientific Research Projects Coordination Units of Bilecik Şeyh Edebali University (Project No: 2022-02.BŞEÜ.01-01) and Gazi University (Project Code: FPD-2024-8919).

During the preparation of this work, the authors used ChatGPT in order to improve several important aspects of writing, such as readability, grammar, spelling, and tone of the text. After using this tool, the authors reviewed and edited the content as needed and take full responsibility for the content of the publication.

DATA AVAILABILITY STATEMENT

Data are available from the corresponding author upon reasonable request.

ORCID

Ömer Mercimek https://orcid.org/0000-0002-5367-6077
Özgür Anıl https://orcid.org/0000-0002-1939-0366

REFERENCES

1. Koutas LN, Tetta Z, Bournas DA, Triantafillou TC. Strengthening of concrete structures with textile reinforced mortars: state-of-the-art review. J Compos Constr. 2019;23(1):3118001.
2. Triantafillou TC, Papanicolaou CG, Zissimopoulos P, Laourdekis T. Concrete confinement with textile-reinforced mortar jackets. ACI Struct J. 2006;103(1):28.
3. Bournas DA, Lontou PV, Papanicolaou CG, Triantafillou TC. Textile-reinforced mortar versus fiber-reinforced polymer confinement in reinforced concrete columns. ACI Struct J. 2007;104(6):740.
4. Basalo FJDC, Matta F, Nanni A. Fiber reinforced cement-based composite system for concrete confinement. Constr Build Mater. 2012;32:55–65.
5. Raoof SM, Bournas DA. TRM versus FRP in flexural strengthening of RC beams: behaviour at high temperatures. Constr Build Mater. 2017;154:424–37.
6. Raoof SM, Koutas LN, Bournas DA. Textile-reinforced mortar (TRM) versus fibre-reinforced polymers (FRP) in flexural strengthening of RC beams. Constr Build Mater. 2017;151:279–91.
7. Cai G, Tsavdaridis KD, Larbi AS, Purnell P. A simplified design approach for predicting the flexural behavior of TRM-strengthened RC beams under cyclic loads. Constr Build Mater. 2021;285:122799.
8. Elsanadedy HM, Almusallam TH, Alsayed SH, Al-Salloum YA. Flexural strengthening of RC beams using textile reinforced mortar–experimental and numerical study. Compos Struct. 2013;97:40–55.
9. Pohoryles DA, Melo J, Rossetto T. Combined flexural and shear strengthening of RC T-beams with FRP and TRM:

experimental study and parametric finite element analyses. Buildings. 2021;11(11):520.
10. Irshidat MR, Al-Shannaq A. Using textile reinforced mortar modified with carbon nano tubes to improve flexural performance of RC beams. Compos Struct. 2018;200:127–34.
11. Mercimek Ö, Anıl Ö, Akkaya ST, Erdem RT, Çelik A, Fener M, et al. Seismic failure analysis of TRM-strengthened shear-critical RC beams under hysteretic loading. Eng Fail Anal. 2025;165:109757. https://doi.org/10.1016/j.engfailanal.2025.109757
12. Tzoura E, Triantafillou TC. Shear strengthening of reinforced concrete T-beams under cyclic loading with TRM or FRP jackets. Mater Struct. 2016;49:17–28.
13. Triantafillou TC, Papanicolaou CG. Shear strengthening of reinforced concrete members with textile reinforced mortar (TRM) jackets. Mater Struct. 2006;39:93–103.
14. Escrig C, Gil L, Bernat-Maso E, Puigvert F. Experimental and analytical study of reinforced concrete beams shear strengthened with different types of textile-reinforced mortar. Constr Build Mater. 2015;83:248–60.
15. Tetta ZC, Koutas LN, Bournas DA. Shear strengthening of concrete members with TRM jackets: effect of shear span-to-depth ratio, material and amount of external reinforcement. Compos Part B Eng. 2018;137:184–201.
16. Tetta ZC, Bournas DA. TRM vs FRP jacketing in shear strengthening of concrete members subjected to high temperatures. Compos Part B Eng. 2016;106:190–205.
17. Azam R, Soudki K. FRCM strengthening of shear-critical RC beams. J Compos Constr. 2014;18(5):4014012.
18. Daneshvar K, Moradi MJ, Roshan N, Noel M, Hajiloo H. Enhancing flexural and shear capacities of RC T-beams with FRCM incorporating a full FRCM-concrete bond. Constr Build Mater. 2025;471(14068):7.
19. Mercimek Ö. Experimental and analytical investigation of the effects of anchor types and strip shapes on shear-deficient reinforced concrete beams strengthened with TRM versus FRP. Int J Civil Eng. 2023;21(12):1927–50.
20. Mercimek Ö, Celik A, Ghoroubi R, Anil Ö. Retrofitting of squat RC column by using TRM strip under axial load. Structures. 2024;60:105909 Elsevier.
21. Bournas DA, Triantafillou TC, Papanicolaou CG. Retrofit of seismically deficient RC columns with textile-reinforced mortar (TRM) jackets. 4th Colloquium on Textile Reinforced Structures (CTRS4). 2009:471–90.
22. Zhou C, Wang W, Zheng Y, Cheng Y, Wu Z. Response and shear mechanism of RC bridge piers confined with CFRP grid-reinforced ECC subjected to truck collision. Eng Fail Anal. 2023;143:106882.
23. Kobbekaduwa D, Nanayakkara O, Di Sarno L, Krevaikas T. Strengthening and repair of deficient reinforced concrete columns using textile-reinforced mortar: state-of-the-art review. Structures. 2024;65:106739.
24. Guo L, Deng M, Li T. Seismic behaviour of RC columns retrofitted with textile-reinforced mortar (TRM) optimized by short PVA fibres. Structures. 2023;50:244–54.
25. Azdejkovic LD, Triantafillou TC. Seismic retrofit of RC short columns with textile-reinforced alkali-activated or cement-based mortars. J Compos Constr. 2023;27(5):4023041.
26. Bournas DA, Triantafillou TC, Zygouris K, Stavropoulos F. Textile-reinforced mortar versus FRP jacketing in seismic retrofitting of RC columns with continuous or lap-spliced deformed bars. J Compos Constr. 2009;13(5):360–71.
27. Mercimek Ö, Ghoroubi R, Özdemir A, Anil Ö, Erbaş Y. Investigation of strengthened low slenderness RC column by using textile reinforced mortar strip under axial load. Eng Struct. 2022;259:114191.
28. Raoof SM, Koutas LN, Bournas DA. Bond between textile-reinforced mortar (TRM) and concrete substrates: experimental investigation. Compos Part B Eng. 2016;98:350–61.
29. D'Ambrisi A, Feo L, Focacci F. Experimental analysis on bond between PBO-FRCM strengthening materials and concrete. Compos Part B Eng. 2013;44(1):524–32.
30. D'Antino T, Pellegrino C, Carloni C, Sneed LH, Giacomin G. Experimental analysis of the bond behavior of glass, carbon, and steel FRCM composites. Key Eng Mater. 2014;624:371–8.
31. Zhang M, Luo Q, Du Y, Deng M, Zhao S. Bond performance of carbon textile reinforced mortar with short fibers for strengthening concrete elements. Case Stud Constr Mater. 2024;21:e03614.
32. Ombres L. Analysis of the bond between fabric reinforced cementitious mortar (FRCM) strengthening systems and concrete. Compos Part B Eng. 2015;69:418–26.
33. D'Antino T, Sneed LH, Carloni C, Pellegrino C. Influence of the substrate characteristics on the bond behavior of PBO FRCM-concrete joints. Constr Build Mater. 2015;101:838–50.
34. Awani O, El Refai A, El-Maaddawy T. Bond characteristics of carbon fabric-reinforced cementitious matrix in double shear tests. Constr Build Mater. 2015;101:39–49.
35. Tran CTM, Stitmannaithum B, Ueda T. Investigation of the bond behaviour between PBO-FRCM strengthening material and concrete. J Adv Concrete Technol. 2014;12(12):545–57.
36. Sneed LH, D'Antino T, Carloni C. Investigation of bond behavior of PBO fiber-reinforced cementitious matrix composite–concrete interface. ACI Mater J. 2014;111(5):569–80.
37. Mercimek Ö. Seismic failure modes of masonry structures exposed to Kahramanmaraş earthquakes (Mw 7.7 and 7.6) on February 6, 2023. Eng Fail Anal. 2023;151:107422.
38. Tan M, Avşar Ö, Yıldızhan F, Atmaca N. Effect of infill walls on the seismic performance of a severely damaged substandard RC building during the February 6, 2023, Kahramanmaras earthquake sequence. Eng Fail Anal. 2025;169:109117.
39. Kazaz İ, Avşar Ö, Dilsiz A. Importance of building inspection on the seismic response of a severely damaged RC structure during the February 6, 2023 Kahramanmaraş earthquake sequence. Eng Fail Anal. 2024;162:108410.
40. İnce O. Structural damage assessment of reinforced concrete buildings in Adıyaman after Kahramanmaraş (Türkiye) earthquakes on 6 February 2023. Eng Fail Anal. 2024;156:107799.
41. Altunsu E, Güneş O, Öztürk S, Sorosh S, Sarı A, Beeson ST. Investigating the structural damage in Hatay province after Kahramanmaraş-Türkiye earthquake sequences. Eng Fail Anal. 2024;157:107857.
42. Doğruyol M. Characterisation of acrylic copolymer treated concretes and concretes of reinforced concrete buildings collapsed in the 6 February 2023 Mw= 7.8 Kahramanmaraş (Türkiye) earthquake. Eng Fail Anal. 2024;161:108249.

43. Ozturk M, Arslan MH, Korkmaz HH. Effect on RC buildings of 6 February 2023 Turkey earthquake doublets and new doctrines for seismic design. Eng Fail Anal. 2023;153:107521.
44. Çalışkan Ö, Yüncüler M, Mercimek Ö, Anıl Ö. Interface failure in TRM–concrete systems with cementitious fan-type anchors under direct tension. Eng Fail Anal. 2025;177:109679.
45. European Committee for Standardization. Testing hardened concrete – Part 3: Compressive strength of test specimens (EN 12390-3). London, UK: CEN; 2019.
46. Blaber J, Adair B, Antoniou A. Ncorr: open-source 2D digital image correlation matlab software. Exp Mech. 2015;55(6):1105–22. https://doi.org/10.1007/s11340-015-0009-1
47. The MathWorks, Inc. MATLAB (Version R2021a) [Computer software]. 2021. https://www.mathworks.com/products/matlab.html
48. Tetta ZC, Koutas LN, Bournas DA. Textile-reinforced mortar (TRM) versus fiber-reinforced polymers(FRP) in shear strengthening of concrete beams. Compos Part B Eng. 2015;77:338–48.
49. ABAQUS User's Manual, Version 6.12. France: SIMULIA, Dassault SystèmesSimulia Corp; 2015.
50. Yılmaz T, Kıraç N, Anil Ö, Erdem RT, Sezer C. Low velocity impact behavior of rc two way slab strengthening with CFRP strips. Constr Build Mater. 2018;186:1046–63.
51. Dönmez TÜ, Türer A, Anil Ö, Erdem RT. Experimental and numerical investigation of timber formwork beam under different loading type. Mech Based Design Struct Mach. 2022;50(3):1090–110.
52. Erdem RT. Experimental and numerical study of fiber reinforced concrete beams in four-point bending. Cem Wapno Beton. 2021;26(5):431–43.
53. Birtel V, Mark P. Parameterised finite element modeling of RC beam shear failure. Proceedings ofthe 19th Annual International ABAQUS Users' Conference, Boston, 95–108. 2006.
54. Mander JB, Priestley MJN, Park R. Theoretical stress–strain model for confined concrete. J Struct Eng. 1989;114(8):1804–26.
55. Obeidat YT, Heyden S, Dahlblom O. The effect of CFRP and CFRP/concrete interface models when modelling retrofitted RC beams with FEM. Compos Struct. 2010;92(6):1391–8.
56. Li C, Hao H, Bi K. Numerical study on these ismic performance of precast segmental concrete columns under cyclic loading. Eng Struct. 2017;148:373–86.

AUTHOR BIOGRAPHIES

Ömer Mercimek is an associate professor in the Department of Civil Engineering at Ankara University, Ankara, Türkiye. His research focuses on seismic performance and strengthening of reinforced concrete and masonry structures, and structural performance of 3D printed concrete walls. Email: omercimek@ankara.edu.tr.

Özlem Çalışkan is an associate professor in the Department of Civil Engineering at Bilecik Şeyh Edebali University, Bilecik, Türkiye. Her research primarily focuses on concrete and reinforced concrete structures. She has contributed to experimental and analytical studies on structural systems. Email: ozlem.caliskan@bilecik.edu.tr.

Özgür Anıl is a professor in the Department of Civil Engineering at Gazi University, Ankara, Türkiye. His research interests mainly involve impact loading, structural response under dynamic effects, and seismic performance evaluation of reinforced concrete systems. He has conducted analytical and experimental studies on structural behavior under extreme loading conditions. Email: oanil@gazi.edu.tr.

R. Tuğrul Erdem is a professor in the Department of Civil Engineering at Manisa Celal Bayar University, Türkiye. His research mainly focuses on impact effects, earthquake engineering, and performance-based assessment of reinforced concrete structures. He has extensive experience in structural safety evaluation and advanced numerical modeling. Email: tugrul.erdem@cbu.edu.tr.

Murat Yüncüler is a Ph.D. student in the Department of Civil Engineering at Bilecik Şeyh Edebali University, Bilecik, Türkiye. His research interests include reinforced concrete systems and strengthening. Email: yunculer.murat@gmail.com.

How to cite this article: Mercimek Ö, Çalışkan Ö, Anıl Ö, Erdem RT, Yüncüler M. TRM-to-concrete interface bond without anchors: Combined experimental, analytical, and numerical modeling approach. Structural Concrete. 2026. https://doi.org/10.1002/suco.70552